博士論文

A novel technique of tracing AMPA receptor endocytosis and recycling in cultured neurons

（AMPA 受容体エンドサイトーシスの新規可視化方法の開発）

林　　亜矢子

Contents

Abstract

Techniques of visualizing receptor trafficking are important, but currently available methods are limited in their labeling efficiency, specificity and reliability. Here I developed a novel labeling method based on peptide-binding-peptide pairs. In this system, membrane proteins tagged with a ZIP-binding cassette at their extracellular domain were expressed on the cell surface and labeled with exogenously applied ZIP peptides conjugated with fluorescent dyes. Surface labeling by ZIP peptides was of low background and high affinity. I applied ZIP peptides tagged with a pH-sensitive dye 4-RhPM to cultured hippocampal neurons and visualized AMPA receptor (AMPAR) internalization. The majority of the AMPAR-containing endocytotic vesicles were localized to PSD-95-positive large spines. Application of 4-RhPM-tagged ZIP peptides induced rapid and synchronized increase of fluorescence signals within individual spines with a half time of 31 s. This observation suggests continuous endocytosis of cell surface AMPARs and subsequent acidification in the endocytotic vesicles that reside within spines. The acidic vesicular pool of AMPARs within spines was distinct from the early endosomes labeled by transferrin uptake. The appearance of AMPARs to the cell surface from the local intracellular pool was estimated by using fluorescence photobleaching of AMPARs tagged with superecliptic pHluorin. The rate of local AMPAR recycling to the cell surface was comparable with the rate of its endocytosis within spines. My results indicate an important role of the endosomal vesicular pool within spines that supports continuous recycling of AMPARs.

Introduction

The number, distribution and modulation of cell surface receptors are main determinants of cellular responses to extracellular signals [1-3]. Receptors bind their ligands generally at neutral pH on the cell surface. The fate of receptors after ligand binding is multiple, but some undergo endocytosis [4]. Immediately after endocytosis, the endocytotic vesicles rapidly decrease intra-vesicular pH by V-type H^+-ATP-dependent proton pumps (V-ATPases) [5]. The receptors are dissociated from ligands in acidic environment, and either sorted to the degradation pathway or recycled back to the plasma membrane for multiple events of ligand binding. The synthesis and trafficking of each receptor protein is a complex process and the regulatory mechanisms of receptor trafficking have not yet been fully understood, as tracing the entire cell surface mobility and vesicular transport of receptors is technically demanding.

To understand the mechanisms of transport, accumulation, and recycling of neurotransmitter receptors, it is important to monitor distribution and movement of receptors both on the cell surface and within intracellular vesicles. This requires tools that distinguish receptor distribution on the surface from that in the intracellular space. Conventional techniques of surface receptor labeling by antibodies have various limitations (Fig.1, Table 1). An immunogloblin G (IgG) isotype of antibodies is of relatively large size (about 150 kDa) and may cause steric hindrance [6-8]. Receptor cross-linking by bi-functional IgG molecules was reported to induce perturbation of surface mobility and internalization of receptors (Fig. 1A) [9,10]. Numerous studies utilize GFP molecules for the detection of receptors (Fig. 1B); however, the molecular mass of GFP (about 27 kDa) may still affect molecular functions. More importantly,

cell surface fluorescence cannot be separated from intracellular signals. To overcome this problem, pH-sensitive GFP, superecliptic pHluorin (SEP), was attached to the extracellular domain of receptors and used to detect cell surface receptors, as its fluorescence was quenched in intracellular acidic compartments [11,12]. Although SEP can detect cell surface receptors and exocytotic events, it cannot monitor the acidic endocytic vesicles and the origin and fate of receptors before and after exocytosis. Recently, improved surface labeling methods have been reported (Table 1) [13-18]. These techniques utilize various interaction partners and chemical modification principles to achieve selective and high affinity labeling of cell surface receptors. These new labeling methods are promising, but both potentials and limitations of these techniques in real experimental settings have not yet been fully explored.

To achieve selective, high-affinity and reliable labeling of cell surface receptors, a novel tag system is required. Researches on coiled-coil peptides indicate their potentials as high affinity tags (Fig. 1C). One candidate is the ZIP peptide pair (Fig. 1D). Their sequences are originally derived from the human B-ZIP leucine zipper protein and modified to improve the affinity and specificity of heterodimerization [19]. Its component peptides, ZIP(+) (5.5 kDa) and ZIP(−) (5.4 kDa) form a heterodimer (Fig. 1E) that is 25 times smaller than antibodies. They bind their targets with high affinity, with K_d of 1.3×10^{-11} M [19,20]. The heterodimerization of the monovalent ZIP(−) / ZIP(+) peptides should not cause aggregation of the molecules of interest. Furthermore, ZIP peptides can be easily conjugated with fluorescent dyes at their termini using either amine-reactive or thiol-reactive groups, because ZIP peptide sequences do not contain lysine (K) and cysteine (C) residues (Fig. 1D).

Using the ZIP system, it would be possible to visualize endocytosis and

distinguish receptors localized on the cell surface from those in the acidic endosomes in combination with pH-sensitive labels. The extracellular domain of membrane proteins is exposed to neutral pH environment and endocytosis of membrane proteins induces rapid decline of pH, due to the activity of endosomal V-ATPases. Several pH-sensitive dyes with increased fluorescence at acidic pH, such as CypHer5E [21], BCECF (Life Technologies), and pHrod [22] , have been developed. These probes are not ideal for monitoring acidification within endosomes, due to their high background signals at neutral pH and insufficient photostability. A newly developed pH-sensitive dye 4-RhPM (RhPM) is derived from rhodamine, contains piperazines in the structure, and is designed to be pH-sensitive through photo-induced electron transfer mechanisms [23]. RhPM is superior for monitoring vesicle dynamics with a higher fluorescence-activation ratio, compared with previously reported pH-sensitive dyes.

Glutamate receptors mediate excitatory synaptic transmission in the vertebrate brain. Glutamate receptors can be classified into the following two broad categories: (1) ligand-gated ionotropic receptors that open directly after glutamate binding, and (2) G protein-coupled metabotropic receptors (mGluRs) that indirectly regulate ion channels through the production of second messengers. The three representative agonists of ionotropic glutamate receptors are AMPA, NMDA and kainate, and receptors are classified by their affinity to these agonists. Most of the glutamatergic synapses contain AMPA receptors (AMPARs) that open with fast kinetics at the resting membrane potential. The NMDA receptors contribute to the slow phase of excitatory postsynaptic current and are blocked by Mg^{2+} ions at the resting membrane potential. AMPARs play a major role in the expression of synaptic plasticity, such as long-term potentiation [24,25]. This process is thought to be driven by either the modulation of synaptic

AMPARs by phosphorylation or insertion of new AMPARs from intracellular pools into the postsynaptic membrane [26]. Several lines of evidences suggest that AMPAR density is regulated by trafficking mechanisms such as receptor exocytosis. Multiple transport mechanisms, including vesicular trafficking through Golgi apparatus, membrane insertion, lateral diffusion on the plasma membrane, endosomal recycling, and receptor degradation may influence the content of synaptic AMPARs [17,27]. In addition, rapid AMPAR insertion and removal to and from the postsynaptic membrane should be considered [28,29]. The comprehensive description of AMPAR transport and recycling in living neurons has not yet been achieved.

Membrane protein recycling is a multi-stage process; membrane proteins are first internalized into coated vesicles, which are subsequently fused to sorting endosomes. Within sorting endosomes, local accumulation of cargo molecules within membrane domains takes place. Retromer-mediated sorting recycles cargos to the cell surface [30]. Cargos destined to degradation process are sorted to the invagination of endosomal membrane by ESCRT (endosomal sorting complexes required for transport) complex to form multivesicular bodies [31]. Other cargos are transported to the trans-Golgi network via retrograde pathway. In addition, there exists recycling endosome-mediated transport of cargos to the cell surface either directly or indirectly through the trans-Golgi network. Although the endosomal trafficking has been extensively studied in non-neuronal models, such as fibroblasts and epithelial cells, our knowledge on the endosomal trafficking in neurons is limited. AMPAR internalization in neurons occurs via clathrin-mediated endocytosis and endocytic zones are observed at dendritic spines [32]. The clathrin adaptor complex AP-2 and dynamin mediate the coupling of endocytotic zones to the postsynaptic density (PSD) [28,33,34]. In addition,

AMPAR endocytosis requires direct binding of the GluA2 cytoplasmic tail to AP-2. Small Rab GTPases, Rab4, Rab5, Rab11, and their effectors, have been shown to regulate endosomal trafficking in dendrites. Rab5 regulates sorting of early endosome whereas Rab4 and Rab11 are involved in endosomal recycling back to the plasma membrane [35,36]. AMPARs undergo endo/exocytosis on a relatively rapid time scale [29]. Once transported by exocytosis to the surface of the dendritic shafts or spines, AMPARs diffuse laterally into the postsynaptic density [37,38].

To monitor membrane receptor recycling, I developed a robust and rapid tagging system using ZIP peptides. To test this system, I monitored receptor recycling in multiple cell types including neurons. I expressed the AMPAR subunit GluA1 tagged with a ZIP-binding cassette in primary hippocampal neurons, which was visualized by the labeling of AMPARs with ZIP peptides conjugated to RhPM. I was able to monitor AMPARs recycling at large PSD-95-positive dendritic spines. My results indicate that by using the ZIP system, I can overcome multiple shortcomings of other available membrane protein labeling systems. The ZIP system is a useful tool for real-time tracking of receptor recycling.

Materials and Methods

All experimental procedures were carried out in compliance with the institutional guidelines of the University of Tokyo and the government of Japan. Every effort was made to minimize the suffering and the number of animals used.

Plasmid construction

A cDNA construct comprising mGluR1a containing an extracellular tag insertion site was generated by inserting an *NheI-XhoI* site at residue 33 downstream of the predicted signal sequence of mGluR1a. Oligonucleotide pairs encoding a high-affinity peptide 2 (HAP2)-tag with a glycine tetramer linker were annealed and then ligated to the NheI-XhoI site. The coding sequence of ZIP was generated using PCR from artificially synthesized ZIP(+) and ZIP(−) DNA (GeneScript). The respective sequences of ZIP(+) , ZIP(−) , and 2HA-ZIP(+) (N-terminal HA (Hemagglutinin) tag followed by C-terminal ZIP(+) tag) are as follows:

ZIP(+):

5′-CTGGAGATCGAGGCCGCCTTCCTGGAGAGGGAGAACACCGCCCTGGAGA
CCAGGGTGGCCGAGCTGAGGCAGAGGGTGCAGAGGCTGAGGAACAGGGTG
AGCCAGTACAGGACCAGGTACGGCCCCCTGGGCGGCGGCAAG,-3′

ZIP(−):

5′-CTGGAGATCAGGGCCGCCTTCCTGAGGCAGAGGAACACCGCCCTGAGGA
CCGAGGTGGCCGAGCTGGAGCAGGAGGTGCAGAGGCTGGAGAACGAGGTG
AGCCAGTACGAGACCAGGTACGGCCCCCTGGGCGGCGGCAAG-3′.

2HA-ZIP(+):

5’-GGTACCGGGGTGGTGGAGGTGGTTACCCATACGACGTGCCAGACTACGC
TGGTTATCCGTATGATGTACCTGATTATGCAGGTGGTGGAGGTGGTCTGGAG
ATCGAGGCCGCCTTCCTGGAGAGGGAGAACACCGCCCTGGAGACCAGGGTG
GCCGAGCTGAGGCAGAGGGTGCAGAGGCTGAGGAACAGGGTGAGCCAGTA
CAGGACCAGGTACGGCCCCCTGGGTGGTGGTAAGGGTGGTGGAGGTGGTGA
ATTC-3’

2HA is a tandem repeat of HA tag motif with amino acid sequence of YPYDVPDYAGYPYDVPDYA.

To obtain 2HA-ZIP(+)-mGluR1, 2HA-ZIP(+) was amplified by PCR using the following primers including a *NheI* and a *XhoI* site at their 5’- and 3’-ends respectively with intervening three glycine residues as flexible linkers and inserted to *NheI/XhoI* site of mGluR1.

The sequences of primer pair are as follows:

5’-AGCTAGCTGGAGGTGGTTACCCATACGACGT-3’

5’-ACTCGAGTCCACCACCCTTACCACCACCC-3’

To obtain 2HA-ZIP(+)-GluA1/2, 2HA-ZIP(+) was amplified by PCR using the following primers including a *NheI* and a *XhoI* site at their 5’- and 3’-ends respectively with intervening three glycine residues as flexible linkers and inserted to *NheI* site of GluA1 and GluA2. The *NheI* restriction site was created after Phe 260 of GluA1 and 2HA-ZIP cassette was inserted at this site. The GluA2 clone RB14 was used to generate 2HA-ZIP-GluA2. The *NheI* restriction site was created after Ser 387 of GluA2 and 2HA-ZIP cassette was inserted at this site.

The sequences of primer pair are as follows:

5’- CGCTAGCAGGTGGTTACCCATACGACGTGCCAG-3’

5’- TGCTAGCAATCCACCACCCTTACCACCACCCAGG -3’

DNA sequences were optimized for the codon usage of rodent cells. The tagged receptor sequences were inserted into mammalian expression vectors with either CMV, β-actin or CAG promoters. Expression plasmid for phytochrome-based near-infrared fluorescent protein (iRFP) (plasmid 31857 deposited by Dr.V. Verkhusha, Addgene, Cambridge, MA) was used for transfection of neurons and subsequent imaging. Plasmids encoding GFP-Rab5 and GFP-Rab11a were provided from Dr. Kajiho and Dr. Katada. Generation of PSD-95-GFP was previously described [39]. DsRed2 was purchased from Clontech (Invitrogen).

Protein purification and fluorescent labeling

The DNA fragments encoding ZIP(−) or ZIP(+) sequences were inserted into pGEX4T-1 (Life Technologies) using *BamHI/NotI* site. *E. coli* (BL-21(DE3)) was transformed with either ZIP(−)-pGEX4T-1 or ZIP(+)-pGEX4T-1 plasmids. Expression of GST-tagged ZIP(−) or GST-tagged ZIP(+) was induced for 3 h with isopropyl-β-D-thiogalactopyranoside (Wako) to a final concentration of 1 mM. They were affinity purified using glutathione-Sepharose 4B (Life Technologies) and reacted with thrombin at 4°C for 12 h to remove the GST tag. The yield of each peptide was approximately 1 mg from 1800 ml of culture. The ZIP(−) peptide was labeled at its lysine or cysteine residues with either succinimidyl ester or maleimide reactive groups conjugated with fluorescent moieties. The purified peptide (10 mg/ml) was reacted with

5 μl of 1.2 mM 6-carboxyfluorescein N-succinimidyl ester (Biochemika), Cy3 N-succinimidyl ester (GE Healthcare), or 50.7 μl of 10 mM RhPM- succinimidyl ester (provided from Dr. Y. Urano) in DMSO for 1 h at room temperature. Fluorophore-labeled ZIP(−) peptides were purified using a PD10 column (GE Healthcare). Labeling efficiency and purity was determined by separating unbound dye with Tricine-SDS–PAGE and subsequent visualization using the gel doc 2000 Gel Documentation System (Bio-Rad) with an optical TRI-acetyl cellulose band-pass BPB-53 filter (Fujifilm). The same SDS-PAGE gels were stained with CBB and scanned using an image scanner (GT-9800F, Epson). The absorbance and the reversibility of ZIP(−)-RhPM were measured using a UV2450 UV-VIS Spectrophotometer (Shimadzu). The pH dependency was measured using a Corona Grating Microplate Reader SH-8000(Lab) (Corona Electric, Japan). CVS-ERA-15mer-fluorescein and CVS 29mer-fluorescein peptides were synthesized by TORAY research center with 80% purity.

Peptide sequences of small tag peptides were as follows:

HAP2: WRYYESSLLPYPDGGGG

CVS-ERA-15mer: YTIWCDIFTNSRGKR

ZIP(+): LEI EAAFLER ENTALET RVAELRQ RVQRLRN RVSQYRT RYGPLG GGK

ZIP(−): LEI RAAFLRQ RNTALRT EVAELEQ EVQRLEN EVSQYET RYGPLG GGK

Reagents for cell culture and immunocytochemistry

For culturing non-neuronal cell lines, Dulbecco's modified Eagle's medium (DMEM, Sigma-Aldrich) and fetal calf serum (FCS, Biowest) were used. For primary neuron culture, the following reagents were used: penicillin–streptomycin (Life Technologies); GlutaMAX (Life Technologies); MEM (Life Technologies), HBSS (Life Technologies); Deoxyribonuclease I from bovine pancreas (Sigma-Aldrich); 2.5% trypsin (Life Technologies); poly L-lysine (Sigma-Aldrich). A different FCS product (SFB 30-732) was used for culturing dissociated neurons. For immunocytochemistry, the following primary antibodies were used: anti-clathrin monoclonal antibody (Thermo Scientific, MA1-065), anti-HA-tag rabbit polyclonal antibody (MBL, 561), anti-GluA1 rabbit polyclonal antibody (Chemicon, AB1504), anti-mGluR1 antibody (provided from Dr. Ryuichi Shigemoto) and anti-fluorescein/Oregon green rabbit antibody (Life Technologies, A889). Primary antibodies were detected by the following secondary antibodies: Cy3-conjugated affinity purified goat anti-rabbit IgG (heavy and light chains) (Jackson ImmunoResearch, 77015) or Alexa Fluor 633-conjugated goat anti-mouse IgG (heary and light chains) (Invitrogen, A21071). In addition, the following reagents were used for immunocytochemistry: control IgG isolated from rabbit serum (Sigma-Aldrich, 18440), glutaraldehyde (Nacalai Tesque), paraformaldehyde (Sigma-Aldrich), and Triton-X-100 (Sigma-Aldrich).

Cell culture

HEK293 and NIH3T3 cells were maintained in DMEM, supplemented with 10% FCS (Biowest S1820), 2% GlutaMAX, 50 U/ml penicillin and 50 mg/ml streptomycin (Sigma-Aldrich) at 37°C in a humidified atmosphere containing 5% CO_2.

When the cells grew to 80% confluence, they were transfected with plasmids containing cDNAs encoding fluorescent probes according to the manufacturer's instructions (Lipofectamine Plus, Life Technologies).

Cultures of dissociated hippocampal neurons

Dissection and dissociation of embryonic mouse hippocampal neurons were performed according to the published methods [40,41] with a minor modification. In brief, hippocampal neurons were prepared from ICR mouse embryos at embryonic day 16.5. The hippocampi were dissected, treated with protease and DNase, and dissociated. Cells were plated onto poly-L-lysine (1 mg/ml) coated glass-bottom dishes (MatTek) at a density of 150–300 cells / mm^2. Cells were maintained in Minimum Essential Medium (MEM) with 2% B18 supplement, 1 mM L-glutamine and 5.5% FCS (SFB 30-732, Hyclone AWA94563), at 37°C in a cell culture incubator with 5% CO_2. Two days after plating, 5 μM cytosine β-D-arabinofuranoside was added to the medium to inhibit glial cell proliferation.

Astrocyte culture

Astrocyte culture was performed according to procedures described by McCarthy et.al[42] with a minor modification. In brief, the hypothalami of C57BL/6J mice (postnatal day 5-9 or 40-50) were dissected, treated with 0.4% DNase, dissociated using 0.25% trypsin EDTA (Sigma-Aldrich), and plated at a density of 5×10^6 cells / 75 cm^2 flask in DMEM supplemented with 10% FCS, 1 mM pyruvate, and 2 mM glutamine. Subsequent feeding was carried out using DMEM plus 10% FCS. After 10 days, the flask was shaken mechanically at 250 rpm overnight on a horizontal orbital

shaker (BR-43FL, TAITEC, Japan), and a top layer of cells, containing oligodendrocyte progenitors, was removed. One day after this purification step, secondary astrocyte cultures were established by trypsinizing the primary culture and sub-plating onto collagen-percolated plastic dishes in DMEM plus 10% FCS.

Transfection

Transient transfection of HEK293 cells and NIH3T3 cells were performed with Lipofectamin Plus Reagent (Life Technologies) according to the manufacturer's instructions. For immunocytochemical or morphological analysis of hippocampal neurons, cells were transfected using a modified calcium phosphate method as previously described [43]. For each 35-mm culture dish, 8 μg of plasmid DNA was used to transfect cells at DIV (days in vitro) 5. DNA-$CaCl_2$ solution (75 μl) was added drop-wise to HEPES-buffered saline with gentle vortexing to a final volume of 150 μl, and incubated for 15 min at room temperature. After replacing the original culture medium with 1.5 ml of serum-free transfection medium, this $CaPO_4$/DNA solution was added drop-wise into culture dishes. After incubation at 37°C for 1 h in a humidified atmosphere containing 5% CO_2, the medium was changed with 10% serum-free transfection medium pre-equilibrated with CO_2 to dissolve the residual $CaPO_4$/DNA precipitate. After incubation for 15 min at 37°C in an atmosphere containing 5% CO_2, the medium was replaced with the original medium.

Protein extraction, Tricin-SDS–PAGE and ZIP protein western blotting

The cell lysates were centrifuged at 15,000 × *g* for 10 min at 4°C. Supernatants were collected and protein concentration was measured using a Pierce 660 nm Protein

Assay Kit (Thermo Scientific). Equal amounts of protein samples were mixed with 4× SDS buffer and denatured for 5 min at 95°C for subsequent experiments. To extract proteins, cultured cells were rinsed twice with PBS and directly lysed with a suitable volume of preheated 2× SDS sample buffer. Cell lysates were harvested and denatured for 5 min at 95°C. For western blotting, proteins were separated on 10% SDS–PAGE gels, and transferred onto a PVDF membrane (Millipore) using a submerged transfer apparatus. Membranes were blocked with 5% skim-milk/TBS solution for 1 h at room temperature and incubated with anti-mGluR1 or anti-GFP antibodies overnight at 4°C. Following incubation with primary antibodies, membranes were washed, incubated with HRP-conjugated secondary antibodies, and visualized using an enhanced chemiluminescence reagent (Life Technologies).

Immunocytochemistry

Cells were washed in PBS, fixed in 2% or 4% PFA in PBS for 25 min at room temperature, and permeabilized in 0.2% Triton X-100 for 5 min. To reduce nonspecific antibody binding, 5% normal goat or horse serum in PBS was added to the cells for 30 min followed by incubation with primary antibodies in PBS for 30 min at room temperature. After washing in PBS, samples were incubated with Alexa Fluor 488 or Cy3-conjugated secondary antibodies (Life Technologies) in PBS for 30 min. Cells were washed in PBS thrice and examined using an S100 inverted microscope (Carl Zeiss, Oberkochen, Germany), an FV1000 confocal microscope (Olympus, Japan), or an IX81 inverted microscope (Olympus, Japan).

Cell labeling

Lysotracker labeling

Neurons were incubated with culture medium containing 5 μM LysoTracker Green (Life Technologies) at 37°C for 2 min, followed by washing out the dye twice with imaging solution.

Fura2 staining

Cells were incubated with imaging solution, including 5 μM Fura-2 AM (Life Technologies) and 0.5% BSA as a carrier at room temperature for 30 min, followed by washing out the dye thrice with imaging solution.

Transferrin (Tf) uptake assay

Neurons were starved for Tf for 2 h in imaging solution followed by incubation with 300 μg/ml Alexa-Tf (Invitrogen) for 1 h at 37°C to label recycling endosomes. The unbound Alexa-Tf was washed off using 2 mg/ml of unlabeled holo-Tf (Sigma-Aldrich).

Fluorescent labeling using ZIP(−)

Neurons were incubated with culture medium or imaging solution, including 3 μg/ml fluorescent-labeled ZIP(−)-peptide at 37°C for 1 h or at room temperature for 10 min, followed by washing out the dye thrice with imaging solution. Pitstop 2 was from abcam.

Microscopy

Confocal microscopy

Fluorescence images were acquired using an inverted Olympus FV1000 confocal microscope or a widefield microscope with an EMCCD camera (iXon3,

Andor). Images were taken by using an oil-immersion 60× objective lens (PL APO, Olympus N.A. 1.4). Morphometric analysis and quantification were performed using ImageJ (NIH) and Metamorph software (Molecular Devices). Segments of non-primary dendrites were selected from each neuron for analyses. Spines were defined as 0.5–2 μm-long dendritic protrusions. The number of spines per unit length of dendrites was determined.

Total internal reflection fluorescence (TIRF) microscopy

An objective lens-type TIRF microscope was built using an Olympus inverted microscope (IX81) equipped with a 488 nm Ar-laser (IMA100, Melles Griot) and a 561 nm solid-state laser (JUNO 561 nm, SOC Japan). A 100× objective lens (UApo N, Olympus, N.A. 1.49) was used. Excitation lasers of 488 and 561 nm wavelengths were reflected by a dichroic mirror (Di01-R405/488/561/635, Semrock) and images were detected using an EMCCD camera (iXon3, Andor) at the side port.

Photobleaching experiments

I bleached a large portion (200 × 400 pixels, corresponding to the sample field of 83 μm × 166 μm) of dendrites. The distance from the soma to the center of the bleached area was 172 $\pm$ 23 μm. Recovery from photobleaching was monitored using image acquisitions at 0.5 Hz with 200 sec duration and normalized to the fluorescence measured before photobleaching. Recovery curves were corrected for the extent of photobleaching within 200 sec and the background fluorescence was subtracted.

Data and statistical analysis

To measure fluorescence intensity of transfected cells, cells expressing DsRed or iRFP were identified, outlines of cells were determined, and intensities within the

boundaries were measured. All data are expressed as the mean plus standard error of the mean (S.E.M.) unless otherwise indicated. Statistical analyses were conducted using GraphPad Prism software. Comparisons between two groups were assessed using a two-tailed unpaired Student's t test; comparisons among multiple groups were evaluated using one-way analysis of variance (ANOVA) followed by Tukey's post-hoc test. P values are indicated in all figures as follows: *$p < 0.05$, **$p < 0.01$.

Results

Labeling of cell surface receptors by the ZIP system

ZIP(−) peptides synthesized in *E. coli* were conjugated with several fluorescent dyes, including fluorescein, Cy3, and RhPM. The purity of the ZIP(−) peptide was estimated to be 87.5% and the fluorescein-labeling efficiency was >95% (Fig. 2A and B). To determine optimal reaction time for labeling living cells, HEK293 cells transfected with ZIP(+)-tagged mGluR1 were incubated with fluorescein-conjugated ZIP(−). Fluorescein-conjugated ZIP(−) at 3 μg/ml decorated surface ZIP(+)-tagged mGluR1 within 5–10 min (Fig. 2C). Labeling efficiencies of three different tagging systems, ZIP(−) / ZIP(+) peptide pairs, αBTx / high-affinity-peptide 2 (HAP2) pairs [44], and a 15mer peptide derived from rabies virus glycoprotein (CVS-ERA-15mer) / HAP2 pairs [45], were compared by measuring fluorescence intensity of living cells expressing mGluR1 fused to binding motifs at the N-terminal after incubation with respective fluorescein-conjugated small peptides (Fig. 2D). Anti-mGluR1 immunocytochemistry confirmed comparable expression levels of mGluR1 fused to different binding motifs. Labeling intensity of fluorescein-conjugated ZIP(−) peptides was similar to that of fluorescein-labeled αBTx (Fig. 2E). Normalized intensity of cells incubated with fluorescein-conjugated CVS-ERA-15mer was lower than that of ZIP(−) peptides (Fig. 2E). These results suggest that ZIP-based labeling is as sensitive as other peptide-based protein detection techniques. Incubation of cells expressing ZIP(−)-tagged mGluR1 with fluorescein-conjugated ZIP(−) peptides did not provide specific surface staining of the transfected cells. Paraformaldehyde fixation did not impair surface labelling by fluorescein-conjugated ZIP(−) peptides (Fig. 2F).

Receptors move rapidly across the cell surface [32,38,46] and stable binding of

fluorescence-labeled tags to cell surface receptors and minimal effects on their distribution are required. To estimate dissociation rates of ZIP(−) peptides, fixed HEK293 cells expressing mGluR1 tagged with either ZIP(+) or HAP2 were labeled with ZIP(−)-Cy3 or αBTx-Alexa Fluor 555, and the time-dependent decrease of surface signal was quantitated (Fig. 3A). Initial high frequency imaging of 20 frames at 0.2 Hz did not decrease fluorescence signals, suggesting that the same irradiation dose with lower imaging frequency (10 min intervals, total duration of 200 min) can be applied for the quantitative analyses of probe dissociation. Fluorescence signals of αBTx-Alexa Fluor 555 gradually decreased (41% ± 6% at 180 min, Fig. 3B), whereas ZIP(−)-Cy3 did not show time-dependent decrease (87% ± 9% at 180 min, Fig. 3C). Retention of fluorescence signals of ZIP(−)-Cy3 at acidic pH (= 5.4) was comparable to that at neutral pH (Fig. 3D). Although labeling of cell surface mGluR1 with divalent antibodies induced receptor clustering (anti-HA in Fig. 3E) [9], this effect was negligible in the case of monovalent binding pairs of ZIP(−) / ZIP(+) peptide pairs and αBTx / HAP2 pairs.

Specific binding of ZIP peptides by the hydrophobic interaction between a glutamate (E) and an arginine (R) residue (Fig.1D) has been shown to be affected by molecules expressed on the cell surface [47]. I tested whether the ZIP-based labeling can be applied to primary neurons and astrocytes. Neurons and astrocytes expressing ZIP(+) tagged mGluR1 were successfully labeled with ZIP(−)-Cy3, while ZIP(−)-Cy3 did not show specific labeling of neurons expressing ZIP(−) tagged mGluR1 (Fig. 4).

Receptor-mediated endocytosis visualized by pH-sensitive fluorescence probes conjugated to the ZIP peptide

The ZIP-tag system may be useful for monitoring receptor endocytosis because binding is maintained under acidic conditions. I labeled ZIP(−) peptide with an acidic pH-activatable fluorescence probe RhPM-SE (Fig. 5A). The wavelength of maximum absorption of ZIP(−)-RhPM was 542 nm (Fig. 5B). ZIP(−)-RhPM fluorescence increased 7.3 fold from pH 7.4 to 5.5 (17.96 a.u. to 130.3 a.u., Fig. 5C and D) with fast activation kinetics (Fig. 5E) and high photostability (Fig. 5F), which are advantages for live cell imaging. Labeling of fixed HEK293 cells expressing ZIP(+)-tagged mGluR1 with ZIP(−)-RhPM and subsequent quantitative fluorescence imaging confirmed pH-dependency of surface label (Fig. 5G) and reversibility of fluorescence signal by repetitive exposure to the acidic pH (Fig. 5H, I). Live imaging of HEK293 cells expressing ZIP(+)-tagged mGluR1 and subsequent labeling with ZIP(−)-RhPM revealed punctate fluorescent signals, which may reflect endocytotic vesicles. To confirm the properties of structures positive with ZIP(−)-RhPM, I labeled acidic vesicles with Lysotracker and confirmed colocalization of intracellular structures positive with ZIP(−)-RhPM with a fraction of membrane components positive with Lysotracker (Fig. 5J-L). These results indicate that the ZIP system is a useful tool for monitoring receptor internalization.

Visualization of internalized AMPARs in hippocampal neurons using ZIP-based labeling

Monitoring AMPAR dynamics is critical for understanding fast synaptic transmission in neuron. The ZIP(+) peptide was coupled to the N-terminus of the AMPAR subunit GluA1 (ZIP(+)-GluA1), expressed in cultured hippocampal neurons, and detected by fluorescently labeled ZIP(−) peptide. Confocal microscopy of

ZIP(−)-Cy3-labeled neurons expressing ZIP(+)-GluA1 revealed specific surface labeling of the somatodendritic compartment, which was not detected in neurons expressing ZIP(−)-GluA1 (Fig. 6A). In my transfection conditions, exogenously expressed ZIP(+)-GluA1 did not influence the staining intensities of anti-GluA1 antibody and the distribution of GluA1 clusters along dendrites (Fig. 6B and C), suggesting minimal interference in total GluA1 distribution in transfected neurons.

By switching fluorophores from Cy3 to RhPM, I aimed at selective labeling of AMPARs after endocytosis and acidification of the early endosomes. Hippocampal neurons transfected with both SEP-GluA1 and ZIP(+)-GluA1 were labeled with ZIP(−)-RhPM for 1 h. TIRF imaging detected RhPM-positive punctate structures in dendrites. The specificity of the labeling was confirmed by labeling of ZIP(+)-GluA1-expressing neurons with non-binding peptide ZIP(+)-RhPM or labeling of neurons transfected with only SEP-GluA1 and subsequent labeling with ZIP(−)-RhPM (Fig. 6D and E). Treatment of neurons with 1 mM of Pitstop 2 , an inhibitor of clathrin-mediated endocytosis, completely eliminated increase in RhPM fluorescence (Fig. 6F and G). Chemical fixation of ZIP(+)-GluA1 transfected neuron also inhibited increase in RhPM fluorescence (data not shown). I also successfully detected total and internalized GluA2 by the ZIP-based detection method. After labeling with either ZIP(−)-Cy3 or ZIP(−)-RhPM, neurons expressing ZIP(+)-tagged GluA1 or ZIP(+)-tagged GluA2 showed punctate pattern of fluorescence distribution with similar densities (Fig. 6H and I). These data indicate that ZIP(−)-RhPM specifically binds to ZIP(+)-GluA1 and GluA2 and increase its fluorescence after endocytosis and subsequent acidification.

The majority of ZIP-RhPM-labeled GluA1 and GluA2 puncta were present

within dendritic spines (Fig. 7A and B). These data are consistent with a previous analysis using antibody-based detection of AMPAR endocytosis [48]. I classified dendritic protrusions into four morphological categories [49] of mushroom spines, stubby spines, thin spines, and filopodia (Fig. 7C). The proportion of ZIP-RhPM-positive protrusions within each subtype were as follows: 72.5%, mushroom; 47.6%, stubby; 38.7%, thin; 18.8%, filopodia, for neurons expressing ZIP(+)-GluA1 (Fig. 7D and E). Similar proportions of spines positive with RhPM clusters were detected in GluA2-expressing neurons. Large spines were reported to contain more membranous components [48,50-53]. Consistent with these previous observations, relatively large mushroom-type spines had more RhPM-GluA1 clusters (data not shown), suggesting enrichment of GluA1-contining endosomal components.

Rapid switching of extracellular pH (between pH 7.4 and pH 5.4) induced modulation of both SEP-GluA1 and ZIP(−)-RhPM fluorescence in opposite directions (Fig. 8A and B). Fluorescence ratio of ZIP(−)-RhPM at pH 7.4 against pH 5.4 was 53.7 ± 3.5% (Fig. 8C), which may reflect the ratio of ZIP(−)-RhPM-labeled internal and total GluA1. Additionally, application of 50 mM NH_4Cl, which induces neutralization of intracellular vesicles, triggered reduction of RhPM fluorescence intensity (Fig. 8D and E) [54,55]. These results are consistent with the idea that most of the RhPM fluorescence signals are derived from intracellular vesicular pool with acidic pH and the fraction of intracellular endocytosed AMPARs are substantial.

The small size of ZIP peptides and their monovalent property is advantageous for the unperturbed monitoring of cell surface receptors and their endocytosis. To illustrate differences between ZIP-based labeling and antibody-based detection, 2HA-ZIP(+)-GluA1-transfected cells were first reacted with either anti-HA antibodies

or control IgG for 10 min, followed by ZIP(−)-RhPM labeling for another 10 min. I applied the technique of rapid switching of extracellular pH (between pH 7.4 and pH 5.4) again and estimated the ratio of internalized and total GluA1 receptors (Fig. 8F). The estimated internal/total ratio of ZIP-RhPM-labeled GluA1 reduced significantly by prior surface labeling with anti-HA antibodies (Fig. 8G). This observation suggests the possibility of blocking normal endocytotic events by excessive antibody labeling of AMPARs and this inhibitory effect may be less problematic in ZIP-based labeling.

Properties of acidic intracellular vesicles containing RhPM-labeled AMPARs

My quantitation of RhPM puncta within dendrites indicated that the majority of RhPM-labeled AMPARs within acidic intracellular vesicles were located in spines (Fig 7B). In addition, the majority of mushroom-type spines were positive with RhPM-labeled AMPARs (Fig. 7E). AMPARs are transported to the cell surface and reside in both synaptic and extra-synaptic membranes. Active endocytosis of AMPARs has been detected using a variety of labeling techniques. However, these studies did not report extensive labeling of the spine cytoplasm comparable to the level detected by the RhPM-based method I reported in this study. This may be due to the advantageous properties of RhPM-based detection, which is less likely to interfere with the endocytotic events (Fig. 8G) because of its small probe size.

To further clarify the nature of acidic intracellular vesicles detected by RhPM-lableled AMPARs, I first compared localization of RhPM-positive puncta with the localization pattern of SEP-GluA1 and PSD-95-GFP. Distribution of SEP-GluA1 and PSD-95-GFP, which reflects the position of the PSD, should be in close vicinity of RhPM-labeled AMPAR-containing vesicles, but should not be completely overlapped.

Images of living neurons expressing either SEP-GluA1 or PSD-95-GFP together with ZIP(+)-GluA1 and subsequent ZIP(−)-RhPM labeling confirmed partial overlapping of RhPM-positive puncta with either SEP-GluA1 or PSD-95-GFP (Fig. 9A and B). There was a positive correlation between the fluorescence intensities of PSD-95-GFP and those of nearby RhPM-labeled GluA1 (Fig. 9C). These observations are consistent with the idea that the acidic intracellular vesicles containing RhPM-labled AMPARs are in the close vicinity of the PSDs, either within spines or in dendritic shafts.

I next assessed the distribution of endocytosis-related structures within dendrites of culture hippocampal neurons. Immunocyochemistry of clathrin heavy chain revealed clustered immunoreactivity along dendritic shafts (Fig. 9D). Clustered immunoreactivity may reflect accumulation of clathrin heavy chains in either presynaptic cytoplasm or postsynaptic spines. Immunoreactive signals were lower in dendritic shafts, compared with synaptic sites. After formation of endocytosed vesicles, luminal pH is quickly lowered by the V-ATPases. To detect the distribution of acidic vesicles within dendrites, live hippocampal neurons were labeled with Lysotracker Green. Intracellular acidic vesicles should be present in dendritic shafts, spines and presynaptic structures, but the distribution of Lysotracker-positive vesicles was consistent with the pattern of postsynaptic structures (Fig. 9E). This observation may indicate less efficient labeling of recycling synaptic vesicles in the presynaptic compartment by using Lysotracker. Nevertheless the intense spine labeling with Lysotracker suggests the presence of acidic vesicles within spines.

Recycling of endosomes is regulated by Rab proteins, which recruit specific effector proteins to the membrane. Rab5 is a well-characterized member of Rab family proteins and is involved in fusion and remodeling of early endosomes. Transfection of

ZIP(+)-GluA1 and GFP-Rab5 and subsequent labeling with ZIP(−)-RhPM revealed spatial relationship between RhPM-labeled AMPARs within acidic vesicles and Rab5-positive endosomes (Fig. 9F). GFP-Rab5 was present in spines and showed co-localization with RhPM-positive puncta. Transfection of GFP-Rab11, another member of Rab family proteins with preferential interaction with recycling endosomes, results in appearance of GFP-positive vesicles in both dendritic shafts and spines. Partial overlap of GFP-Rab11 and RhPM-positive puncta was detected (Fig. 9F). These results are consistent with the idea that a subset of acidic vesicles containing RhPM-labeled AMPARs associate with Rab5 and Rab11-positive endosomal compartments within spines and dendritic shafts.

Fluorescent-labeled transferrin has been used to monitor endosomal dynamics. Apo-transferrin binds to transferrin receptors and triggers their endocytosis. After internalization, apo-transferrin releases Fe^{2+} and recycles back to the plasma membrane [56]. Uptake and subsequent intracellular trafficking of transferrin have been utilized for endosomal dynamics in neurons and the behavior of transferrin-containing endosomal vesicles has been considered to reflect that of AMPAR-containing endosomal vesicles. To test if endosomal recycling of transferrin receptors and AMPARs shares the same sorting pathway or not, I first labeled cultured neurons with either Alexa Fluor 564-conjugated transferrin or GluA1-positive endosomes with ZIP(−)-RhPM and analyzed the distribution of fluorescent puncta. Distributions of two endosome-related components in both immature (DIV 11) and mature (DIV 18) neurons were compared (Fig.10A-D). In immature neurons, overall distribution patterns of Alexa Fluor 564-conjugated transferrin and RhPM-labeled GluA1 were similar. Transferrin and RhPM-labeled GluA1 signals were mainly present in dendritic shafts (80% of

transferrin-positive puncta and 70% of RhPM-positive puncta). Localization of transferrin-positive endosomes remained within dendritic shafts in mature neurons. However, only 20% of RhPM-labeled GluA1 puncta were localized to dendritic shafts at DIV 18. To evaluate the colocalization of transferrin-positive endosomes and RhPM-labeled GluA1, I next labeled neurons expressing ZIP(+)-GluA1with ZIP(−)-RhPM and Alexa Fluor 488-conjugated transferrin (Fig. 10E and F). In immature neurons, 50% of transferrin-positive endosomes colocalized with RhPM-labeled GluA1. In contrast, mature neurons showed only 20% colocalization of transferrin-positive endosomes and RhPM-labeled GluA1. I therefore conclude that the endosomal recycling monitored by transferrin uptake does not reflect the sorting pathway utilized by endocytosed AMPARs especially after maturation of hippocampal neurons.

Measurement of internalization rate of RhPM-labeled GluA1 in living neurons

An advantage of RhPM-based detection of AMPAR-containing vesicles is its low background. Direct application of ZIP(−)-RhPM to the extracellular solution without subsequent washout can detect fluorescence increase within the cytoplasm after RhPM internalization and acidification. Quantification of fluorescence increase in spines after application of ZIP(−)-RhPM to neurons expressing ZIP(+)-GluA1 provides indispensable information in kinetics of AMPAR endocytosis locally within spines (Fig. 11). The fluorescence intensities increased rapidly after dye addition and fluorescence saturated at 5 min with $\tau_{1/2}$ of 31.4 ± 12.3 s (Fig. 11C). Fluorescence increase within spines was not associated with fusion of vesicles transported into spines from dendritic shafts, indicating that local endocytotic events within spines mainly contribute to the

increase of RhPM fluorescence. There were small, but clear variations in the onset of fluorescence increase (Fig. 11D and E), suggesting the stochastic nature of endocytotic events within individual spines. The kinetics of fluorescence increase is determined by the combination of multiple processes, including binding kinetics of ZIP(−)-RhPM to the surface ZIP(+)-GluA1, frequency of endocytotic events within spines, speed of single endocytotic events, and speed of acidification after endocytosis. Kinetics of ZIP binding to surface receptors and acidification of endocytosed vesicles may obscure individual endocytotic events of surface AMPARs. Although these reservations should be taken into account, rapid increase of RhPM fluorescence with similar rapid kinetics across multiple spines can be explained only by the presence of basal and frequent endocytosis of AMPARs locally within dendritic spines.

Visualization of local exocytotic events of AMPARs in dendrites

To directly measure the amount and dynamics of newly exocytosed receptors, I designed an experiment using photobleaching of surface SEP-GluA1 receptors. If photobleaching areas are small, fluorescence recovery after bleaching reflects both lateral diffusion of receptors and insertion of intracellular receptors. To eliminate the contribution of lateral diffusion, entire dendrites from the proximal to the distal ends was scanned with a strong focused blue light and surface SEP-GluA1 fluorescence was eliminated (Fig. 12A). Subsequently, fluorescence at the distal part of bleached dendrites (>100 μm away from cell body) was monitored for 10 min to detect fluorescence recovery. Consistent with previous work, the recovery of GluA1 at distal dendrites 10 min after bleaching was approximately 10% (Fig.12B and C) [57]. Recovery events were detected as sudden increase of local fluorescence within dendrites.

Recovery spots were present in both dendritic shafts and spines (Fig. 12D and E). Local fluorescence increase was in a step-wise manner (Fig.12E). Some spots disappeared while others persisted. These local fluorescence increases were taken as exocytotic events of SEP-GluA1-containing vesicles. From the time-lapse images, kymographs were generated (Fig. 12E bottom) and the events of GluA1 exocytosis were counted. GluA1 exocytotic events occurred stochastically during the 10 min observation period after bleaching (Fig. 12F) and the timing of exocytotic events were independent of the distance from the soma (Fig.12 H), indicating that exocytosis occurs continuously along entire dendrites(Fig.12 G). Frequent local exocytotic events of AMPAR-containing vesicles are consistent with an idea of local AMPAR recycling in dendrites.

Discussion

Here I report a novel surface labeling method for visualizing membrane proteins and subsequent endosomal trafficking. The ZIP-based labeling offers multiple advantages over available membrane protein labeling systems. The ZIP-tag is much smaller than other molecular tags, including antibodies, fluorescent proteins and αBTx. Heteromeric binding of ZIP peptides is based on 14 α-helical motifs that are wrapped around each other to form a super-helix, promoting tight packing of hydrophobic amino acid side chains [58]. The length of ZIP peptide complex is estimated to be 6.6 nm, similar to typical α-helical polypeptides. Inhibition of protein functions by addition of the ZIP-tag should be less problematic than other probes of larger molecular mass. In addition, proximity of fluorescent tags to the target proteins should be advantageous in superresolution imaging. The affinity of ZIP(−)/ZIP(+)-tags is reported to be higher than that of other peptide-based binding pairs. ZIP peptides are an improved version of the original heterobinding peptides derived from B-ZIP proteins [19]. This property may help long lasting labeling of membrane proteins. I confirmed this advantage by comparing the decay of fluorescence signals after surface labeling of fixed cells (Fig. 3A-D). Unaltered dissociation rate of ZIP-based binding at lower pH shown in Figure 3D is another advantage for the retention of probes in acidic intracellular membrane compartments.

The pH activatable dye RhPM, in combination with ZIP peptides, may be useful in faithful monitoring of endocytosed membrane proteins and their intracellular transport and sorting. I could monitor internalization of mGluR1 tagged with ZIP(+) motif by surface labeling with RhPM-labeled ZIP(−) peptides (Fig. 5J-L). In neuronal cells, direct visualization of intracellular trafficking of receptor molecules is required to

understand the mechanisms of synapse maintenance, activity-dependent modulation, and pathology. In this study, I provided the evidences for reliable and efficient labeling of endocytosed AMPAR subunits GluA1 and GluA2 by ZIP-based labeling with RhPM (Fig. 6). The ability of ZIP-based labeling technique to monitor internalization and subsequent sorting of AMPARs in living neurons should be indispensable in research of receptor dynamics in neurons.

AMPARs are critical for maintenance and modulation of excitatory synapses. Using RhPM labeled ZIP peptide, rapid appearance of RhPM fluorescence after surface staining of GluA1 was observed (Fig. 11). Since RhPM fluorescence increases 7-fold from acidic to neutral pH environment with rapid kinetics (Fig. 5), this observation suggests rapid endocytosis and subsequent acidification of GluA1 receptors. Analyses of time-lapse images indicated apparent half-time of 31.4 ± 12.3 s in fluorescence increase and saturation within 5 min. Although surface-labeling experiments of fluorescein-labeled ZIP peptides revealed relatively slow kinetics of ZIP binding (Fig. 2C), this discrepancy may be explained by different affinities between fluorescein-conjugated and RhPM-conjugated ZIP(−) peptides or difference in the N-terminal structure between mGluR1 and GluA1. This point should be clarified by future experiments.

I could not detect single endocytotic events in time-lapse imaging. Binding kinetics of ZIP(−) peptides to surface receptors will determine the number of labeled GluA1 molecules incorporated into single clathrin-coated pits. Therefore RhPM molecules internalized by single endocytotic events will increase gradually with time-course restricted by binding kinetics of ZIP(−) peptides. Furthermore, acidification of endocytosed vesicles should not be instantaneous and activation of RhPM within

single endocytosed vesicles should follow the time course of acidification determined by V-ATPase activity. At present, these two critical parameters, the binding kinetics of ZIP(−) peptides and the speed of acidification, are not available. However, it is reasonable to assume that visualization of single endocytotic events at the beginning of time-lapse imaging after application of RhPM-conjugated ZIP(−) peptides should be difficult, due to both initial low labeling of internalized GluA1 and slow kinetics of acidification.

In spite of these limitations, several characteristics of GluA1 endocytosis and acidification monitored by RhPM/ZIP-based labeling is remarkable. Rapid RhPM signals appeared within 5 min in a large fraction of spines, indicating the presence of active endocytotic machinery in the majority of spines. Previous studies of endocytotic activity within spines utilized fluorescently labeled transferrin as a marker of endocytosis. However, recent cell biological studies suggested that trafficking of endocytotic vesicles is cargo-dependent [30]. It is possible that transferrin receptors and AMPARs, two distinct cargo molecules, are internalized and sorted by distinct pathways. My analyses of transferrin uptake clearly showed development-dependent segregation of endosomal pathways between AMPARs and transferrin receptors (Fig. 10), further supporting the presence of distinct sorting pathways. Endocytosis of AMPARs within spines is likely to be dependent on clathrin-mediated process. Previous imaging studies of clathrin dynamics reported the presence of clathrin-mediated endocytosis in both dendritic shafts and spines, but the frequency of clathrin assembly within spines was reported to be suppressed along with differentiation of neurons in culture[59]. The RhPM/ZIP-based labeling revealed rapid increase of internalized GluA1 within 5 min. Importantly, the onset of fluorescence increase in individual spines

was variable (Fig. 11D), suggesting that internalization of AMPARs takes place stochastically with average frequency of 0.2-0.03 Hz in single spines. In summary, the RhPM/ZIP-based labeling revealed new features of AMPAR endocytosis in spines.

RhPM/ZIP-based labeling is a technique useful for tracing the fate of surface receptors after endocytosis. Although I could successfully visualize the initial step of GluA1 endocytosis and acidification within spines, subsequent sorting pathways of the internalized GluA1 receptors could not be detected. Time-lapse imaging of RhPM-labeled internalized GluA1 for extended time periods did not detect transformation of the early endosomal structure into tubular vesicles extending to dendritic shafts nor scission of RhPM-positive vesicles and formation of transport vesicles moving toward dendritic shafts. One possible interpretation of the lack of transport of RhPM-labeled endosomal vesicles from spines to dendritic shafts is the confinement of entire endosomal recycling within spines. In this case, relatively stable fluorescence content in individual spines can be explained by the equilibrium between endocytosis and exocytosis. Although previous electron microscopic studies postulated the presence of vesicular structures related to recycling endosomes within the spine cytoplasm, the fraction of spines containing the entire components of recycling endosomes (clear vesicles, tubular vesicles connected to large vesicles with multivesicular bodies) was relatively small [52,53]. Alternatively, RhPM-labeled AMPARs may move to recycling endosomes within dendritic shafts through tubular endosomal membranes connecting spine heads and dendritic shafts. These tubular membranes are frequently found within the base and neck of spines and postulated to be involved in rapid transport of cargo molecules [60]. These two models should be tested experimentally by developing imaging techniques with high spatial and temporal

resolution that can detect mobility of RhPM-containing individual vesicles within spines.

Photobleaching of a large area of dendritic arborization and subsequent monitoring of fluorescence recovery at the distal dendrites revealed stochastic appearance of punctate SEP-GluA1 fluorescence. These events are likely to be associated with either appearance of recycled SEP-GluA1 or de novo appearance of SEP-GluA1 from the trans-Golgi membrane compartment. These two pathways are difficult to separate, as in both pathways SEP-GluA1 molecules are within acidic environment and escape photobleaching. A kinetic property of SEP-GluA1 exocytosis was distinct from endocytosis in its frequency. Within 10 min period of time-lapse imaging, the number of local exocytotic events was not more than 10, which supplied 10% of the total surface AMPARs (Fig. 12C). Endocytotic events within spines are more frequent and 50% of the total spine AMPARs are transported to the acidic vesicles within 5 min (Fig. 8C and Fig. 11C). These two transport system can be balanced, if I assume the ratio of synaptic and non-synaptic AMPARs on the dendritic surface to be 1:10. Because AMPARs exist on non-synaptic membranes with relatively high density, this ratio of synaptic and non-synaptic AMPARs may be acceptable.

Recently, fluorescent lifetime imaging of pH sensitive dyes was reported [61,62]. It is known that intracellular pH is critical for the protein transport and function. For example, in a mouse model of Angelman syndrome, Golgi apparatus shows an unpacked abnormal pattern due to its luminal neutral pH [63]. The ability to determine accurate pH within organelles such as the Golgi apparatus, endosomes and lysosomes, may provide insight into complex sorting mechanisms and disease-related impairments. Future studies using ZIP-based labeling may reveal its broad application in cell surface

labeling, endosomal trafficking, and regulation of luminal pH.

Figure legends

Figure 1 Relative sizes and primary structures of ZIP peptides

(A–C) Sizes and interactions of different probes to membrane proteins with a putative molecular weight of 130 kDa. Interaction of divalent antibodies with membrane proteins (A) may induce oligomerization and masking of their surface. GFP tagging may be less problematic but reports both intracellular and surface proteins (B). Peptide-binding peptides may be advantageous with their small sizes and a monovalent nature. Scale bar, 2 nm.

(D) The coiled-coil ZIP peptides are 49 amino acids in length and form dimers. The lysine residue at the C-termini of ZIP peptides can be utilized for labeling with NHS-ester.

(E) The coiled-coil ZIP peptides form α-helix and interact with each other by electrostatic interactions of arginine (R) and glutamate (E) residues at the interface.

Figure 2 Purification, fluorescence labeling of ZIP peptides and application in cell surface labeling

(A) SDS-PAGE of ZIP(−) peptide in the purification process. Lane 1, 2: lysate. 3: supernatant (S). 4: pellet (P) after GST purification. 5: pellet after incubation with thrombin. 6, 7: lysate after incubation with 5 μl (lane 6) or 10 μl (lane 7) of thrombin. The ZIP(−) peptide (6 kDa, marked by asterisk) was obtained after cleavage of GST-tagged ZIP(−) peptide (marked by double asterisk).

(B) Tricine-SDS-PAGE of fluorescein-conjugated ZIP(−) peptide (marked by triple asterisk). CBB; the same gel preparation stained with CBB after recording of fluorescence.

(C) Quantification of cell surface intensity of fluorescein-conjugated ZIP(−) at various times after application of the probe to ZIP(+)-mGluR1 transfected HEK293 cells (39 cells, 3 cultures). Data are shown as mean ± SEM.

(D)Surface labeling of peptide-tagged mGluR1-transfected HEK293 cells with four different peptide-based probes. Anti-mGluR1 staining of permeabilized cells confirmed comparable levels of mGluR1 expression. Images were acquired by the widefield microscope. Scale bar, 10 μm.

(E) Quantification of cell surface labeling by four different peptide-based probes. Fluorescence intensities derived from surface peptide probes were normalized by total mGluR1 staining (10 images). Data are shown as mean ± SEM.

(F) Comparison of cell surface labeling with live or fixed preparations transfected with ZIP(+)-mGluR1 and surface labeled by ZIP(−)-fluorescein (red) for 1 h. Images were acquired by the widefield microscope. Scale bar, 10 μm.

Figure 3 Higher stability and reduced clustering of ZIP-based surface labeling

(A) Time course of probe dissociation from cells surface. Fixed HEK293 cells expressing peptide-tagged mGluR1 were reacted with Alexa Fluor 555-labeled αBTx or Cy3-labeled ZIP(−) peptide, washed, and imaged with intervals of 10 min for 200 min with external solution at pH 7.4. Initial high frequency imaging (20 flames at 0.2 Hz)

with same laser intensity confirmed the absence of photobleach. Images were acquired by the confocal microscope. Scale bar, 10 μm.

(B and C) Dissociation time course of Alexa Fluor 555-labeled αBTx (B) or Cy3-labeled ZIP(−) peptide (C) (9 cells, 3 cultures). Data are shown as mean ± SEM.

(D) Fluorescence intensity ratio (180 min / 0 min) was calculated from dissociation time courses shown in (B) and (C). Similar plots were made for the experiments with external solution at pH5.4 (9cells, 3 cultures). Data are shown as mean ± SEM.

(E) Cell surface labeling of HEK293 cells expressing peptide-tagged mGluR1 with fluorescent probes. Higher magnification images confirmed absence of receptor clustering with monovalent αBTx or ZIP(−) peptide. Images were acquired by the widefield microscope. Scale bar, 10 μm.

Figure 4 Detection of mGluR1 in both neurons and glia by ZIP-based labeling

(A) Selective labeling of cell surface ZIP-tagged mGluR1 by appropriate binding partners. Primary hippocampal neurons expressing ZIP(+)-mGluR1 were efficiently labeled by ZIP(−)-Cy3, but neurons expressing ZIP(−)-mGluR1 showed negligible staining. Scale bar, 10 μm. Images were acquired by the confocal microscope.

(B) Successful surface labeling of primary astrocytes expressing ZIP(+)-mGluR1 with ZIP(−)-Cy3. Images were acquired by the widefield microscope. Scale bar, 10 μm.

Figure 5 Characterization of acidic pH-activatable fluorescence probe, 4-RhPM, conjugated with ZIP(−) peptides

(A) Chemical structure of 4-RhPM. 4-RhPM-SE was used for labeling purified ZIP(−) peptides.

(B) Absorption spectrum of the 4-RhPM-labeled ZIP(−) peptides in 200 mM PBS (pH 2.0) containing 5% SDS.

(C) Relationship of fluorescence intensity of 4-RhPM-labeled ZIP(−) peptides to pH.

(D) Comparison of the intensity of ZIP(−)-RhPM at pH 5.4 and at pH 7.4, indicating. 7.2-times increase at pH 5.4 (n = 1).

(E) Increase in fluorescence after rapid change of pH from 5.4 to 7.4. RhPM protonation was induced within 1 s.

(F) Faithful report of repetitive changes in pH between 5.4 (red lines) and 7.4 (blue lines) by fluorescence intensity of ZIP(−)-RhPM (n = 1).

(G) Switching of external pH between 7.4 and 5.4 induced rapid change in cell surface ZIP(−)-RhPM signal. Fixed HEK293 cells expressing ZIP(+)-mGluR1 were labeled with ZIP(−)-RhPM. Images were acquired by the widefield microscope. Scale bar, 10 μm.

(H) Quantification of fluorescence intensity of the cell shown in (G). Open circle represented the neutral condition (pH7.4). Closed circles indicate the acidic condition (pH 5.4).

(I) Quantification of fluorescence intensity at two pH conditions shown in (G) and (H), normalized by the signal at pH 7.4 (5 cells). Data are shown as mean ± SEM.

(J) Colocalization of ZIP(−)-RhPM signals and Lysotracker green in living HEK293 cells. Cells expressing ZIP(+)-mGluR1 were labeled with ZIP(−)-RhPM (red) and

Lysotracker green (green). RhPM-mGluR1 positive puncta colocalized with Lysotracker-labeled acidic vesicles (arrow). Images were acquired by the confocal microscope. Scale bar, 10 μm.

(K) Orthogonal images of the cell shown in (J). Scale bar, 10 μm.

(L) YZ images of the cell shown in (J). Cell boundary detected by iRFP fluorescence was marked by dashed lines. Arrows indicate the intracellular structure marked by arrows in (K). Scale bar, 10 μm.

Figure 6 Detection of cell surface and internalized AMPARs by ZIP-based labeling

(A) Specific labeling of ZIP(+)-GluA1 expressing neurons by ZIP(−)-Cy3 in dissociated hippocampal culture. Images were acquired by the confocal microscope. Scale bar, 10 μm.

(B and C) Total GluA1 in neurons transfected with ZIP(+)-GluA1 estimated by anti-GluA1 immunocytochemistry. A transfected (GFP-positive, arrow) neuron and an untransfected (arrowhead) neuron showed similar levels of GluA1 immunoreactivity. Higher magnification images of dendrites were shown in (C). Images were acquired by the confocal microscope. Scale bars, 100 μm (B), 10 μm (C).

(D) Detection of internalized GluA1 receptors by ZIP(−)-RhPM labeling. ZIP(−)-RhPM reacted with only neurons expressing ZIP(+)-GluA1, but not with control neurons. ZIP(+)-RhPM did not recognize ZIP(+)-GluA1. Images were acquired by the TIRF microscope. Scale bar, 10 μm.

(E) Fluorescence intensity of ZIP(−)-RhPM and ZIP(+)-RhPM, with different combinations of tagged receptors shown in (D) (7 dendrites).

(F) Inhibition of ZIP(−)-RhPM signals by application of 1 mM Pitstop 2. Images were acquired by the TIRF microscope. Scale bar, 10 μm.

(G) Quantitation of puncta intensities after Pitstop 2 treatment shown in (F). The increase in intensity was completely inhibited by Pitstop 2 (control; 29 dendrites, Pitstop 2; 15 dendrites).

(H) Comparable labeling intensity and distribution by RhPM- or Cy3-labeled ZIP(−), after incubation of neurons expressing ZIP(+)-tagged AMPAR subunits. Scale bar, 10 μm. Images were acquired by the TIRF microscope.

(I) Densities of RhPM-GluA1 and -GluA2 clusters along dendrites of labeled neurons (11 dendrites). All data are shown as mean ± SEM.

Figure 7 Presence of internalized AMPARs detected by ZIP(−)-RhPM-based imaging in a majority of spines

(A) Detection of spines positive with internalized AMPARs by labeling ZIP(+)-tagged AMPARs with ZIP(−)-RhPM. Scale bar, 10 μm. Images were acquired by the TIRF microscope.

(B) Proportion of RhPM-positive puncta localized to either spines or dendritic shafts. More than 70% of RhPM –positive puncta were present in spines (GluA1, 10 dendrites; GluA2, 11 dendrites). Data are shown as mean ± SEM.

(C) Morphological subtypes of spines. Schematics of the four standard categories of spines and filopodia. (i) mushroom, (ii) stubby, (iii) thin, (iv) filopodia.

(D) Representative images of the RhPM-GluA1 puncta within spines. Images were acquired by the TIRF microscope. Scale bar, 1 μm.

(E) RhPM-GluA1 or GluA2-positive spines were categorized into four groups shown in (C) and the proportions of RhPM –positive protrusions in each group were calculated (GluA1; 269 protrusion, GluA2; 123 protrusions).

Figure 8 Estimation of intracellular AMPARs by manipulation of external pH

(A) Modulation of fluorescence intensities of SEP-GluA1 and ZIP(−)-RhPM fluorescence in opposite directions by rapid switching of extracellular pH (between pH 7.4 and 5.4). Neurons transfected with SEP-GluA1 and ZIP(+)-GluA1were labeled with ZIP(−)-RhPM for 1 h before imaging. Images were acquired by the TIRF microscope. Scale bar, 10 μm.

(B) Quantification of fluorescence intensity with switching of extracellular pH (from pH 7.4 to 5.4). The intensities were normalized to the first image (circle, SEP-GluA1) or the last image (triangle, ZIP-RhPM labeled GluA1).

(C) Calculation of the ratio of fluorescence intensity at two time points (0 sec vs 60 sec in (A), 39 puncta). Data are shown as mean ± SEM.

(D) Images of SEP-GluA1 and RhPM-labeled GluA1 in neurons maintained in external solution at pH 7.4 and images after switching to external solution with 50 mM NH_4Cl. Images were acquired by the TIRF microscope. Scale bar, 10 μm.

(E) Fluorescence intensities of individual RhPM puncta measured in a neutral pH solution and after replacement with an NH_4Cl–containing solution. (47 puncta, 4 cells)

(F) Prior labeling with anti-HA antibody reduced internalization of 2HA-ZIP(+)-GluA1. AMPAR internalization was detected by subsequent labeling with RhPM-ZIP(−). The extent of cell surface labeling by RhPM-ZIP(−) was estimated by increased fluorescence

after switching of external solution to pH 5.4. Scale bar, 10 μm. Images were acquired by the TIRF microscope.

(G) The extent of AMPAR internalization was estimated by the ratio of RhPM-ZIP(−) signals at two different external pH conditions (intensity at pH 7.4 / intensity at pH 5.4). (control, 5 dendrites; Ab, 6 dendrites). Data are shown as mean ± SEM.

Figure 9 Spatial relationship between RhPM-labeled internalized AMPARs and other postsynaptic and endosomal markers.

(A and B) Distribution of RhPM-labeled internalized GluA1 compared with surface GluA1 and PSD-95. Partial overlap of endocytosed GluA1 and two postsynaptic markers could be detected. Images were acquired by the TIRF microscope. Scale bar, 10 μm.

(C) Correlation between fluorescence intensities of individual PSD-95-GFP puncta and ZIP(−)-RhPM-labeled-GluA1 clusters. (n = 268 puncta, 12 dendrites)

(D) Clathrin heavy chain immunoreactivity in cultured hippocampal neurons. At higher magnifications, clathrin immunoreactivity showed punctate distribution along dendrites, which may reflect its synaptic localization. Images were acquired by the confocal microscope. Scale bars, 50 μm (upper image) and 10 μm (lower image).

(E) Distribution of RhPM-labeled internalized GluA1 (red) compared with Lysotracker green-labeled acidic membrane compartment (green). Some Lysotracker-positive puncta were positive with RhPM-labeled internalized GluA1 (arrows), while other Lysotracker-positive puncta were negative (arrowheads). Images were acquired by the

widefield microscope (Lysotracker green) and the TIRF microscope (RhPM). Scale bar, 10 μm.

(F) Distribution of small GTPases Rab5 and Rab11 in dendrites, in relation to the positions of RhPM-labeled internalized GluA1. Both Rab5 and Rab11 associated with a subset of RhPM-GluA1-positive clusters. Images were acquired by the widefield microscope (iRFP) and the TIRF microscope (GFP and RhPM). Scale bar, 10 μm.

Figure 10 Differential localization of transferrin-positive endosomal vesicles and RhPM-labeled internalized AMPARs

(A) Transferrin-positive endosomes labeled by Alexa Fluor 568 conjugated-transferrin in neurons at DIV 11 and 18. Transferrin-positive endosomes were mainly localized at dendritic shafts. Images were acquired by the widefield microscope (iRFP) and the TIRF microscope (Tf-Alexa568). Scale bar, 10 μm.

(B) Proportion of transferrin-positive endosomes localized to the dendritic shafts and spines at two different culture stages (8 dendrites).

(C) RhPM-labeled internalized GluA1 visualized at DIV 11 and 18. Images were acquired by the widefield microscope (iRFP) and the TIRF microscope (GluA1-RhPM). Scale bar, 10 μm. (D) Proportion of RhPM-labeled internalized GluA1 localized to the dendritic shafts and spines. Distribution of RhPM-labeled internalized GluA1 shifts from dendritic shafts to spines as differentiation proceeds (10 dendrites).

(E) Double labeling of transferrin-positive endosomes and RhPM-labeled internalized GluA1 at DIV 11 and DIV 18. Images were acquired by the widefield microscope (iRFP) and the TIRF microscope (Tf-alexa488 and GluA1-RhPM). Scale bar, 10 μm.

(F) Colocalization of two vesicular compartments (Internalized GluA1 colocalized with transferrin / total internalized GluA1) (8 dendrites). All data are shown as mean ± SEM.

Figure 11 Measurement of GluA1 internalization kinetics

(A) Live imaging of SEP-GluA1 and ZIP(+)-GluA1-transfected neurons after rapid application of ZIP(−)-RhPM. Images were obtained every 5 sec. Images were acquired by the TIRF microscope. Scale bar, 10 μm.

(B) Kymographs of RhPM fluorescence increase. Black arrow head indicates the time point of ZIP(−)-RhPM application. Variability in the onset of fluorescence increase was observed (white arrow heads). Double lines, 50 s. Scale bar, 10 μm.

(C) The averaged fluorescence increase of RhPM-labeled GluA1 puncta (133 puncta).

(D) The initial 10 frames (5 sec intervals) were shown to illustrate the differential onset of RhPM-fluorescence increase. Asterisks indicate the onset of fluorescence increase. Scale bar, 1 μm. Data are shown as mean ± SEM.

(E) The histogram of the first time frames in which ZIP(−)-RhPM puncta were detected (53 events, 3 cells).

Figure 12 Estimation of kinetics and extent of local AMPAR exocytosis by photobleaching of SEP-GluR1

(A) Design of photobleaching experiments for the detection of exocytosis. SEP-GluA1 expressing neurons (left) were selected and a wide bleaching area was set (center) to prevent surface diffusion of AMPARs during time-lapse imaging. After bleaching,

imaging of a small dendritic segment more than 100 μm away from the soma was performed (right).

(B and C) Live imaging of the distal dendrite before, immediately after, and 10 min after bleaching of the entire dendritic arborization for 1 min. Images were acquired by the confocal microscope. Scale bar, 10 μm. The distal dendritic segments recovered about 10% of initial intensity after 10 min (5 dendrites). Data are shown as mean ± SEM.

(D) During the recovery phase from the bleaching, high frequency imaging was performed with increased gain of the photomultiplier. With this imaging configuration local rapid increase of SEP-GluA1-derived signals could be detected. Scale bar, 10 μm.

(E) A line along a dendrite (middle panel) was set and was stretched using ImageJ plug-in. Temporal changes in fluorescence along this line was presented as a kymograph (lower panel). From the kymograph, the onsets of SEP-GluA1 exocytotic events were identified. Scale bar, 10 μm.

(F) A single exocytotic event of SEP-GluA1 (at 45 sec) captured in time-lapse imaging. Scale bar, 10 μm.

(G) The histogram of SEP-GluA1 exocytotic events after photobleaching. Absence of increase in exocytotic events in later time points suggests minimal contribution of slow diffusion of surface receptors from the unbleached proximal dendrites (69 events, 5 cells).

(H) Relationship between the position of SEP-GluA1 exocotytic events and their timing within the observation period. If surface diffusion from proximal dendrites contributes to the generation of SEP-GluA1 puncta, appearance of SEP-GluA1 puncta should be

more frequent in the proximal dendrites at early time points. However, such correlations did not exist (69 events, 5 cells).

Acknowledgements

I would like to express my sincere gratitude to Professor Shigeo Okabe for having accepted me as a Ph-D student and for his supervision. I also warmly thank Professor Yasuteru Urano for his help in application of pH-sensitive fluorescence probes. Finally I would like to thank all the members of the Department of Cellular Neurobiology for their helpful advice and supports.

References

1 Das, S. S. & Banker, G. A. The role of protein interaction motifs in regulating the polarity and clustering of the metabotropic glutamate receptor mGluR1a. *J Neurosci* **26**, 8115-8125, (2006).

2 Kopec, C. D., Real, E., Kessels, H. W. & Malinow, R. GluR1 links structural and functional plasticity at excitatory synapses. *J Neurosci* **27**, 13706-13718, (2007).

3 Craig, A. M., Blackstone, C. D., Huganir, R. L. & Banker, G. The Distribution of glutamate receptors in cultured rat hippocampal-neurons - postsynaptic clustering of AMPA-selective subunits. *Neuron* **10**, 1055-1068, (1993).

4 Bonifacino, J. S. & Traub, L. M. Signals for sorting of transmembrane proteins to endosomes and lysosomes. *Annu Rev Biochem* **72**, 395-447, (2003).

5 Murata, Y. *et al.* Differential localization of the vacuolar H^+ pump with G subunit isoforms (G1 and G2) in mouse neurons. *J Biol Chem* **277**, 36296-36303, (2002).

6 Gonczy, P. *et al.* Functional genomic analysis of cell division in C-elegans using RNAi of genes on chromosome III. *Nature* **408**, 331-336, (2000).

7 Baselga, J. Monoclonal antibodies directed at growth factor receptors. *Annals of Oncology* **11**, 187-190, (2000).

8 Hashida, H. *et al.* The novel monoclonal antibody MH8-4 inhibiting cell motility recognizes integrin alpha 3: inverse of its expression with metastases in colon cancer. *Int J Oncol* **18**, 89-95, (2001).

9 Heine, M. *et al.* Surface mobility of postsynaptic AMPARs tunes synaptic transmission. *Science* **320**, 201-205, (2008).

10 Lin, J. W. *et al.* Distinct molecular mechanisms and divergent endocytotic pathways of AMPA receptors internalization. *Nat Neurosci* **3**, 1282-1290, (2000).

11 Miesenbock, G., De Angelis, D. A. & Rothman, J. E. Visualizing secretion and synaptic transmission with pH-sensitive green fluorescent proteins. *Nature* **394**, 192-195, (1998).

12 Sankaranarayanan, S., De Angelis, D., Rothman, J. E. & Ryan, T. A. The use of pHluorins for optical measurements of presynaptic activity. *Biophys J* **79**, 2199-2208, (2000).

13 Chen, I., Howarth, M., Lin, W. & Ting, A. Y. Site-specific labeling of cell surface proteins with biophysical probes using biotin ligase. *Nat Methods* **2**, 99-104, (2005).

14 Passafaro, M., Piech, V. & Sheng, M. Subunit-specific temporal and spatial patterns of AMPA receptor exocytosis in hippocampal neurons. *Nat Neurosci* **4**, 917-926, (2001).

15 McCann, C. M., Bareyre, F. M., Lichtman, J. W. & Sanes, J. R. Peptide tags for labeling membrane proteins in live cells with multiple fluorophores. *BioTechniques* **38**, 945-952, (2005).
16 Sekine-Aizawa, Y. & Huganir, R. L. Imaging of receptor trafficking by using alpha-bungarotoxin-binding-site-tagged receptors. *Proc Natl Acad Sci U S A* **101**, 17114-17119, (2004).
17 Ehlers, M. D. Reinsertion or degradation of AMPA receptors determined by activity-dependent endocytic sorting. *Neuron* **28**, 511-525, (2000).
18 Griffin, B. A. Specific covalent labeling of recombinant protein molecules inside live cells. *Science* **281**, 269-272, (1998).
19 Moll, J. R., Ruvinov, S. B., Pastan, I. & Vinson, C. Designed heterodimerizing leucine zippers with a range of pIs and stabilities up to 10(-15) M. *Protein Science* **10**, 649-655, (2001).
20 Maruo, T., Ebihara, T., Sato, E., Kondo, S. & Okabe, S. Cre complementation with variable dimerizers for inducible expression in neurons. *J Med Dent Sci* **55**, 247-254, (2008).
21 Beletskii, A. *et al.* High-throughput phagocytosis assay utilizing a pH-sensitive fluorescent dye. *BioTechniques* **39**, 894-897, (2005).
22 Ogawa, M. *et al.* High sensitivity detection of cancer in vivo using a dual-controlled activation fluorescent imaging probe based on H-dimer formation and pH activation. *Mol Biosyst* **6**, 888-893, (2010).
23 Urano, Y. *et al.* Selective molecular imaging of viable cancer cells with pH-activatable fluorescence probes. *Nat Med* **15**, 104-109, (2009).
24 Kessels, H. W. & Malinow, R. Synaptic AMPA receptor plasticity and behavior. *Neuron* **61**, 340-350, (2009).
25 Malinow, R. & Malenka, R. C. AMPA receptor trafficking and synaptic plasticity. *Annu Rev Neurosci* **25**, 103-126, (2002).
26 Liao, D. H., Zhang, X. Q., O'Brien, R., Ehlers, M. D. & Huganir, R. L. Regulation of morphological postsynaptic silent synapses in developing hippocampal neurons. *Nat Neurosci* **2**, 37-43, (1999).
27 Parton, R. G., Simons, K. & Dotti, C. G. Axonal and dendritic endocytic pathways in cultured neurons. *J Cell Biol.* **119**, 123-137, (1992).
28 Carroll, R. C. *et al.* Dynamin-dependent endocytosis of ionotropic glutamate receptors. *Proc Natl Acad Sci U S A* **96**, 14112-14117, (1999).
29 Luscher, C. *et al.* Role of AMPA receptor cycling in synaptic transmission and plasticity. *Neuron* **24**, 649-658, (1999).
30 Hsu, V. W., Bai, M. & Li, J. Getting active: protein sorting in endocytic recycling. *Nat Rev Mol Cell Biol* **13**, 323-328, (2012).
31 Raiborg, C. & Stenmark, H. The ESCRT machinery in endosomal sorting of ubiquitylated membrane proteins. *Nature* **458**, 445-452, (2009).

32 Blanpied, T. A., Scott, D. B. & Ehlers, M. D. Dynamics and regulation of clathrin coats at specialized endocytic zones of dendrites and spines. *Neuron* **36**, 435-449, (2002).
33 Nedivi, E., Hevroni, D., Naot, D., Israeli, D. & Citri, Y. Numerous candidate plasticity-related genes revealed by differential cDNA cloning. *Nature* **363**, 718-722, (1993).
34 Lu, J. *et al.* Postsynaptic positioning of endocytic zones and AMPA receptor cycling by physical coupling of dynamin-3 to homer. *Neuron* **55**, 874-889, (2007).
35 Gerges, N. Z., Brown, T. C., Correia, S. S. & Esteban, J. A. Analysis of Rab protein function in neurotransmitter receptor trafficking at hippocampal synapses. **403**, 153-166, (2005).
36 Hirling, H. Endosomal Trafficking of AMPA-type Glutamate Receptors. *Neuroscience* **158**, 36-44, (2009).
37 Borgdorff, A. J. & Choquet, D. Regulation of AMPA receptor lateral movements. *Nature* **417**, 649-653, (2002).
38 Tardin, C., Cognet, L., Bats, C., Lounis, B. & Choquet, D. Direct imaging of lateral movements of AMPA receptors inside synapses. *EMBO J* **22**, 4656-4665, (2003).
39 Okabe, S., Kim, H. D., Miwa, A., Kuriu, T. & Okado, H. Continual remodeling of postsynaptic density and its regulation by synaptic activity. *Nat Neurosci* **2**, 804-811, (1999).
40 Usui, S. *et al.* Synaptic targeting of PSD-Zip45 (Homer 1c) and its involvement in the synaptic accumulation of F-actin. *J Biol Chem* **278**, 10619-10628, (2003).
41 Okabe, S., Miwa, A. & Okado, H. Alternative splicing of the C-terminal domain regulates cell surface expression of the NMDA receptor NR1 subunit. *J Neurosci* **19**, 7781-7792, (1999).
42 Mccarthy, K. D. & Devellis, J. Preparation of separate astroglial and oligodendroglial cell-cultures from rat cerebral tissue. *J Cell Biol.* **85**, 890-902, (1980).
43 Jiang, M. & Chen, G. High Ca^{2+}-phosphate transfection efficiency in low-density neuronal cultures. *Nat Protoc* **1**, 695-700, (2006).
44 Harel, M. *et al.* The binding site of acetylcholine receptor as visualized in the X-ray structure of a complex between alpha-bungarotoxin and a mimotope peptide. *Neuron* **32**, 265-275, (2001).
45 Kumar, P. *et al.* Transvascular delivery of small interfering RNA to the central nervous system. *Nature* **448**, 39-43, (2007).
46 Blanpied, T. A., Kerr, J. M. & Ehlers, M. D. Structural plasticity with preserved topology in the postsynaptic protein network. *Proc Natl Acad Sci U S A* **105**, 12587-12592, (2008).
47 Ono, S., Yano, Y. & Matsuzaki, K. Improvement of probe peptides for coiled-coil labeling by introducing phosphoserines. *Biopolymers* **98**, 234-238, (2012).

48 Kennedy, M. J., Davison, I. G., Robinson, C. G. & Ehlers, M. D. Syntaxin-4 defines a domain for activity-dependent exocytosis in dendritic spines. *Cell* **141**, 524-535, (2010).
49 Peters, A. & Kaiserman-Abramof, I. R. The small pyramidal neuron of the rat cerebral cortex. The perikaryon, dendrites and spines. *Am J Anat* **127**, 321-355, (1970).
50 Matsuzaki, M. *et al.* Dendritic spine geometry is critical for AMPA receptor expression in hippocampal CA1 pyramidal neurons. *Nat Neurosci* **4**, 1086-1092, (2001).
51 Nusser, Z. *et al.* Cell type and pathway dependence of synaptic AMPA receptor number and variability in the hippocampus. *Neuron* **21**, 545-559, (1998).
52 Cooney, J. R., Hurlburt, J. L., Selig, D. K., Harris, K. M. & Fiala, J. C. Endosomal compartments serve multiple hippocampal dendritic spines from a widespread rather than a local store of recycling membrane. *J Neurosci* **22**, 2215-2224, (2002).
53 Park, M. *et al.* Plasticity-induced growth of dendritic spines by exocytic trafficking from recycling endosomes. *Neuron* **52**, 817-830, (2006).
54 Jaskolski, F., Mayo-Martin, B., Jane, D. & Henley, J. M. Dynamin-dependent membrane drift recruits AMPA receptors to dendritic spines. *J Biol Chem* **284**, 12491-12503, (2009).
55 Ashby, M. C. *et al.* Removal of AMPA receptors (AMPARs) from synapses is preceded by transient endocytosis of extrasynaptic AMPARs. *J Neurosci* **24**, 5172-5176, (2004).
56 Dassler, K., Zydek, M., Wandzik, K., Kaup, M. & Fuchs, H. Release of the soluble transferrin receptor is directly regulated by binding of its ligand ferritransferrin. *J Biol Chem* **281**, 3297-3304, (2006).
57 Petrini, E. M. *et al.* Endocytic trafficking and recycling maintain a pool of mobile surface AMPA receptors required for synaptic potentiation. *Neuron* **63**, 92-105, (2009).
58 Reinke, A. W., Grant, R. A. & Keating, A. E. A Synthetic coiled-coil interactome provides heterospecific modules for molecular engineering. *J Am Chem Soc* **132**, 6025-6031, (2010).
59 Blanpied, T. A., Scott, D. B. & Ehlers, M. D. Dynamics and regulation of clathrin coats at specialized endocytic zones of dendrites and spines. *Neuron* **36**, 435-449, (2002).
60 Wang, Z. *et al.* Myosin Vb mobilizes recycling endosomes and AMPA receptors for postsynaptic plasticity. *Cell* **135**, 535-548, (2008).
61 Kouda K., Kamiya M., Sakurai C., Asanuma D., Wada I. and Urano Y. Rational design of fluorescence probes for measuring pH in acidic vesicles based on fluorescence lifetime imaging. *Annual Meeting of the Pharmaceutical Society of Japan* **133rd**, (2013).

62 Tantama, M., Hung, Y. P. & Yellen, G. Imaging intracellular pH in live cells with a genetically encoded red fluorescent protein sensor. *J Am Chem Soc* **133**, 10034-10037, (2011).
63 Condon, K. H., Ho, J., Robinson, C. G., Hanus, C. & Ehlers, M. D. The Angelman syndrome protein Ube3a/E6AP is required for Golgi acidification and surface protein sialylation. *J Neurosci* **33**, 3799-3814, (2013).
64 Lentz, T. L. Rabies virus binding to an acetylcholine receptor alpha-subunit peptide. *J Mol Recognit* **3**, 82-88, (1990).
65 Harbury, P. B., Zhang, T., Kim, P. S. & Alber, T. A switch between two-, three-, and four-stranded coiled coils in GCN4 leucine zipper mutants. *Science* **262**, 1401-1407, (1993).
66 McCann, C. M., Bareyre, F. M., Lichtman, J. W. & Sanes, J. R. Peptide tags for labeling membrane proteins in live cells with multiple fluorophores. *BioTechniques* **38**, 945-952, (2005).
67 Zhang, Z., Zhu, W. & Kodadek, T. Selection and application of peptide-binding peptides. *Nat Biotechnol* **18**, 71-74, (2000).
68 Los, G. V. *et al.* HaloTag: a novel protein labeling technology for cell imaging and protein analysis. *ACS Chem Biol* **3**, 373-382, (2008).
69 Chen, B., Cao, H., Yan, P., Mayer, M. U. & Squier, T. C. Identification of an orthogonal peptide binding motif for biarsenical multiuse affinity probes. *Bioconjug Chem* **18**, 1259-1265, (2007).

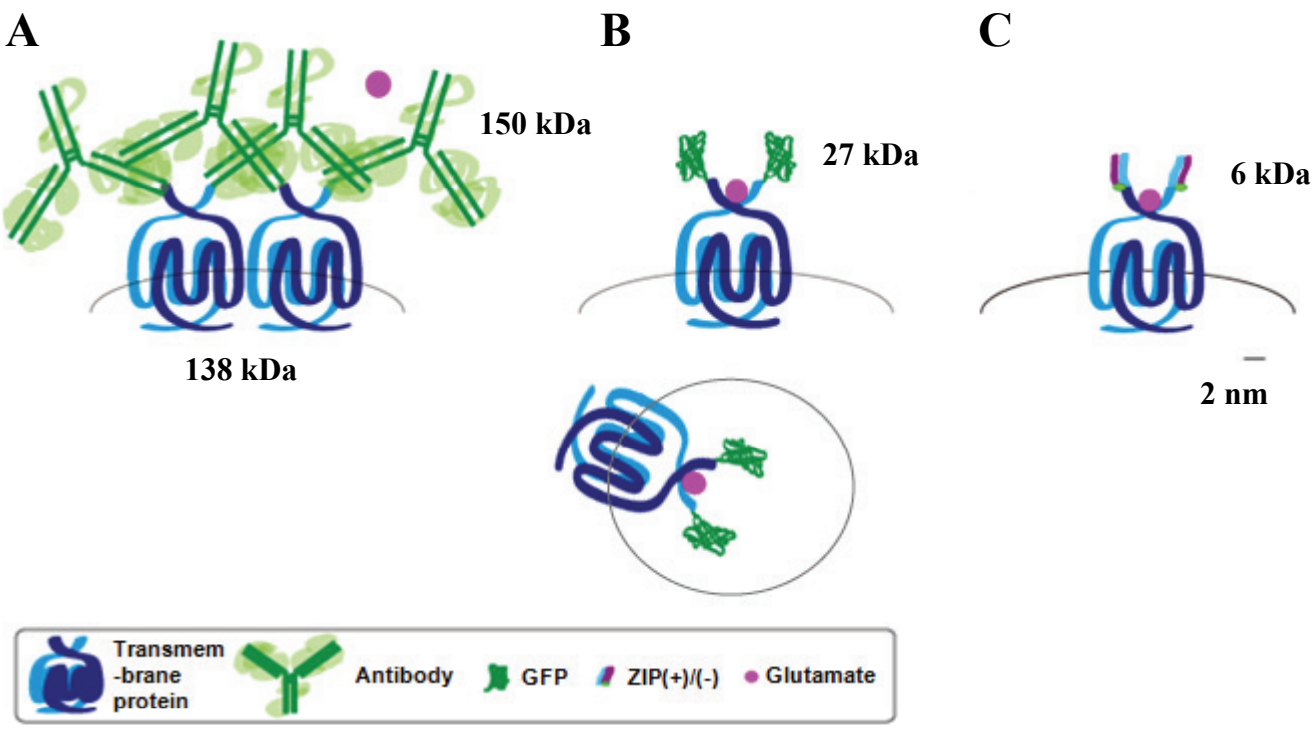

D

ZIP (-) LEIRAAFLRQRNTALRTEVAELEQEVQRLENEVSQYETRYGPLGGGK

ZIP (+) LEIEAAFLERENTALETRVAELRQRVQRLRNRVSQYRTRYGPLGGGK

E

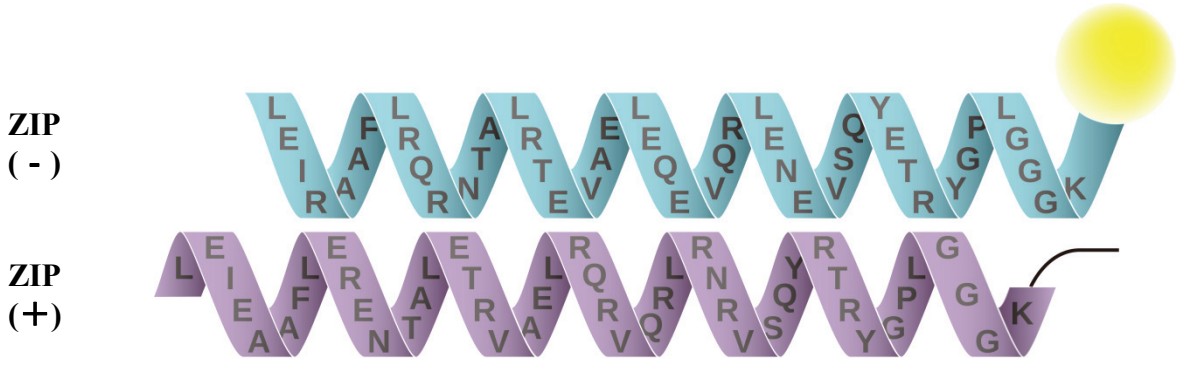

Fig. 1

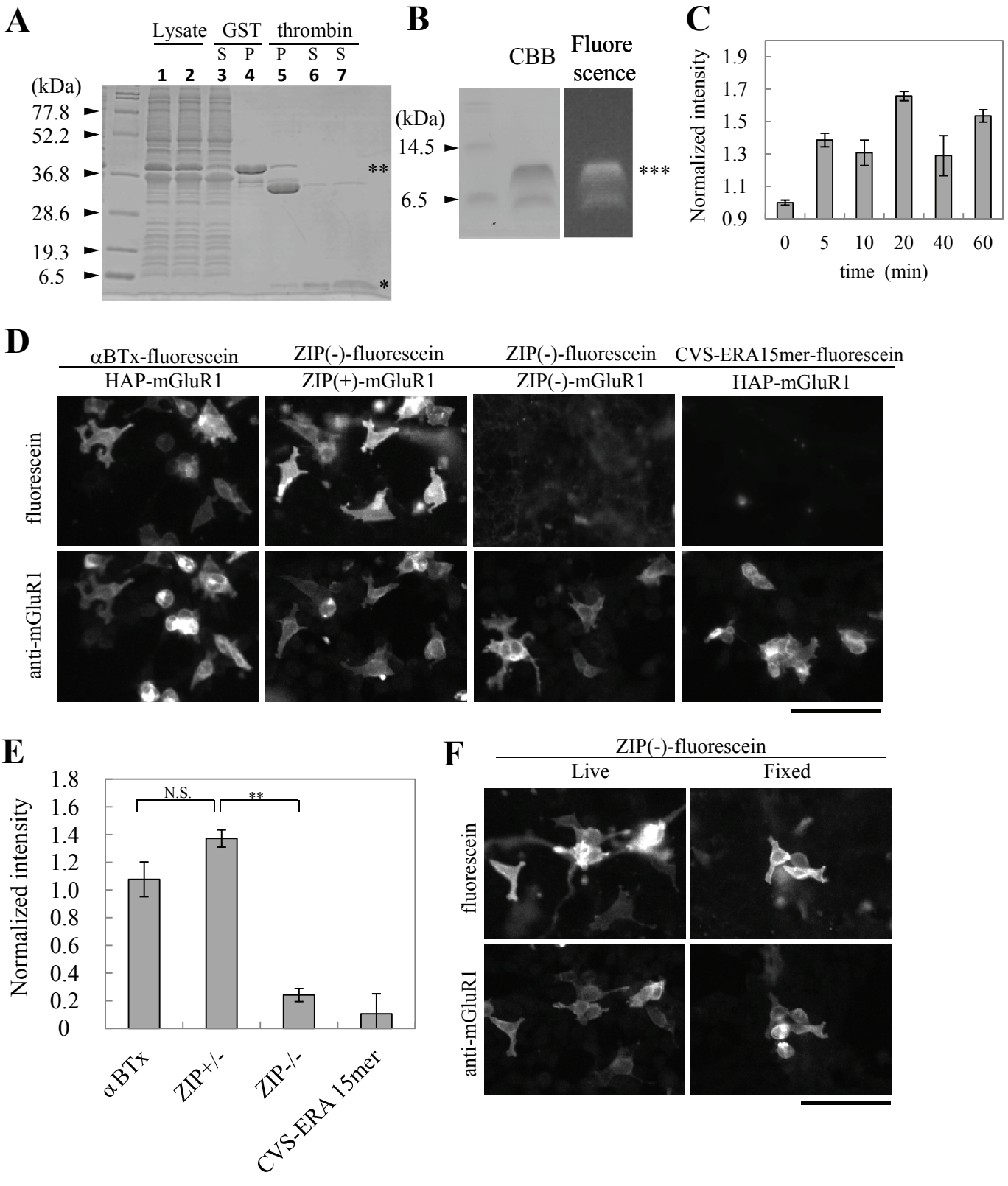
A
Lysate
GST
thrombin
S P P S S
1 2 3 4 5 6 7
(kDa)
77.8
52.2
36.8
28.6
19.3
6.5
**
*
B
CBB
Fluore scence
(kDa)
14.5
6.5
***
C
Normalized intensity
1.9
1.7
1.5
1.3
1.1
0.9
0 5 10 20 40 60
time (min)
D
αBTx-fluorescein
HAP-mGluR1
ZIP(-)-fluorescein
ZIP(+)-mGluR1
ZIP(-)-fluorescein
ZIP(-)-mGluR1
CVS-ERA15mer-fluorescein
HAP-mGluR1
fluorescein
anti-mGluR1
E
Normalized intensity
1.8
1.6
1.4
1.2
1.0
0.8
0.6
0.4
0.2
0
N.S.
**
αBTx
ZIP+/-
ZIP-/-
CVS-ERA 15mer
F
ZIP(-)-fluorescein
Live
Fixed
fluorescein
anti-mGluR1

Fig. 2

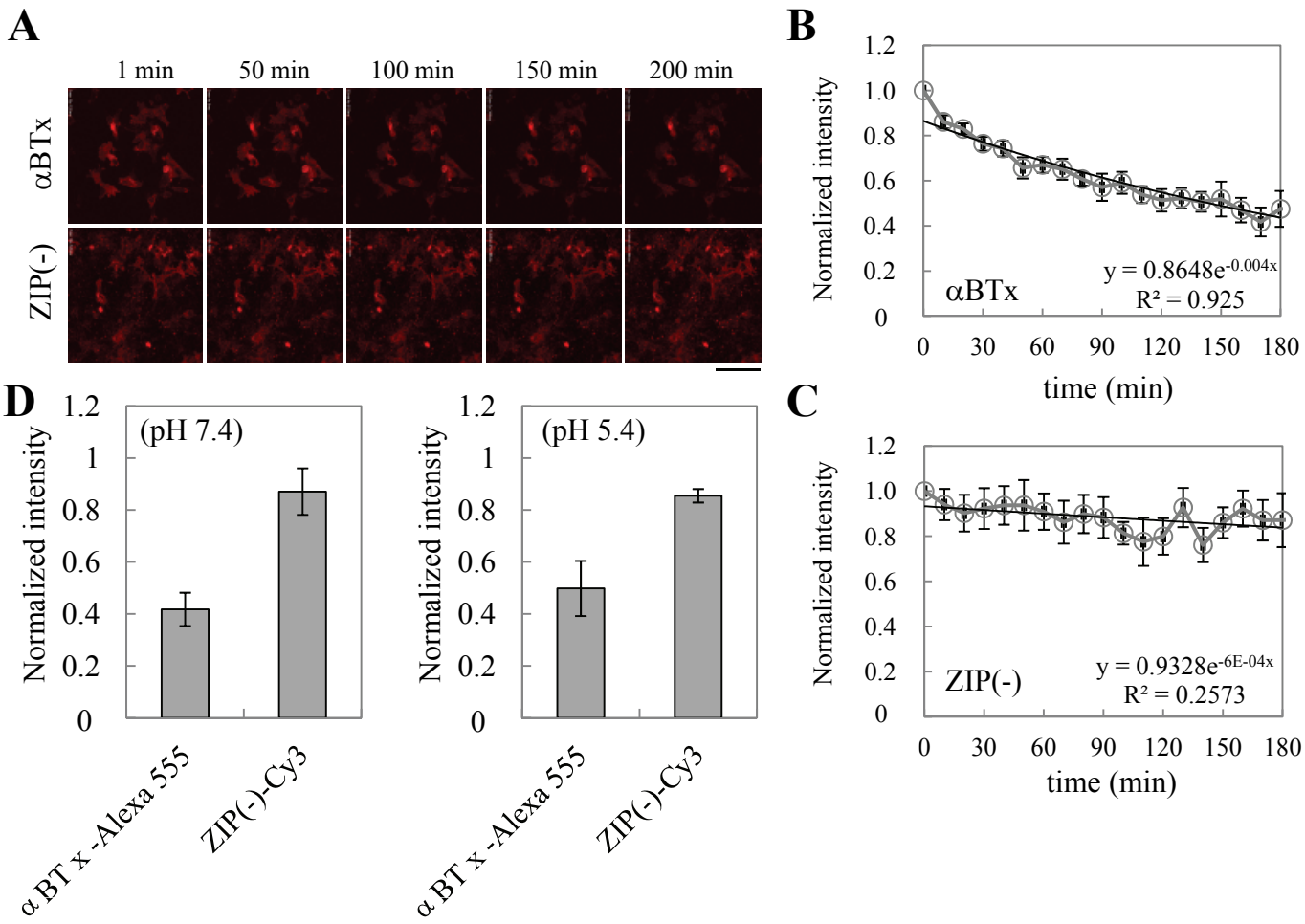
A
1 min
50 min
100 min
150 min
200 min
αBTx
ZIP(-)
B
Normalized intensity
αBTx
y = 0.8648e-0.004x
R² = 0.925
time (min)
C
ZIP(-)
y = 0.9328e-6E-04x
R² = 0.2573
D
(pH 7.4)
(pH 5.4)
α BT x -Alexa 555
ZIP(-)-Cy3

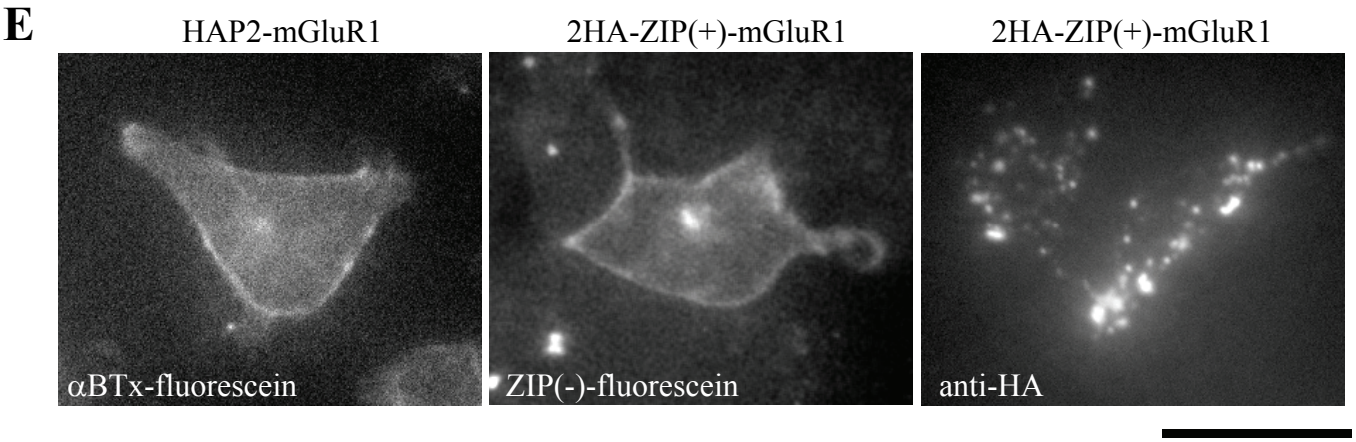
E
HAP2-mGluR1
2HA-ZIP(+)-mGluR1
2HA-ZIP(+)-mGluR1
αBTx-fluorescein
ZIP(-)-fluorescein
anti-HA

Fig. 3

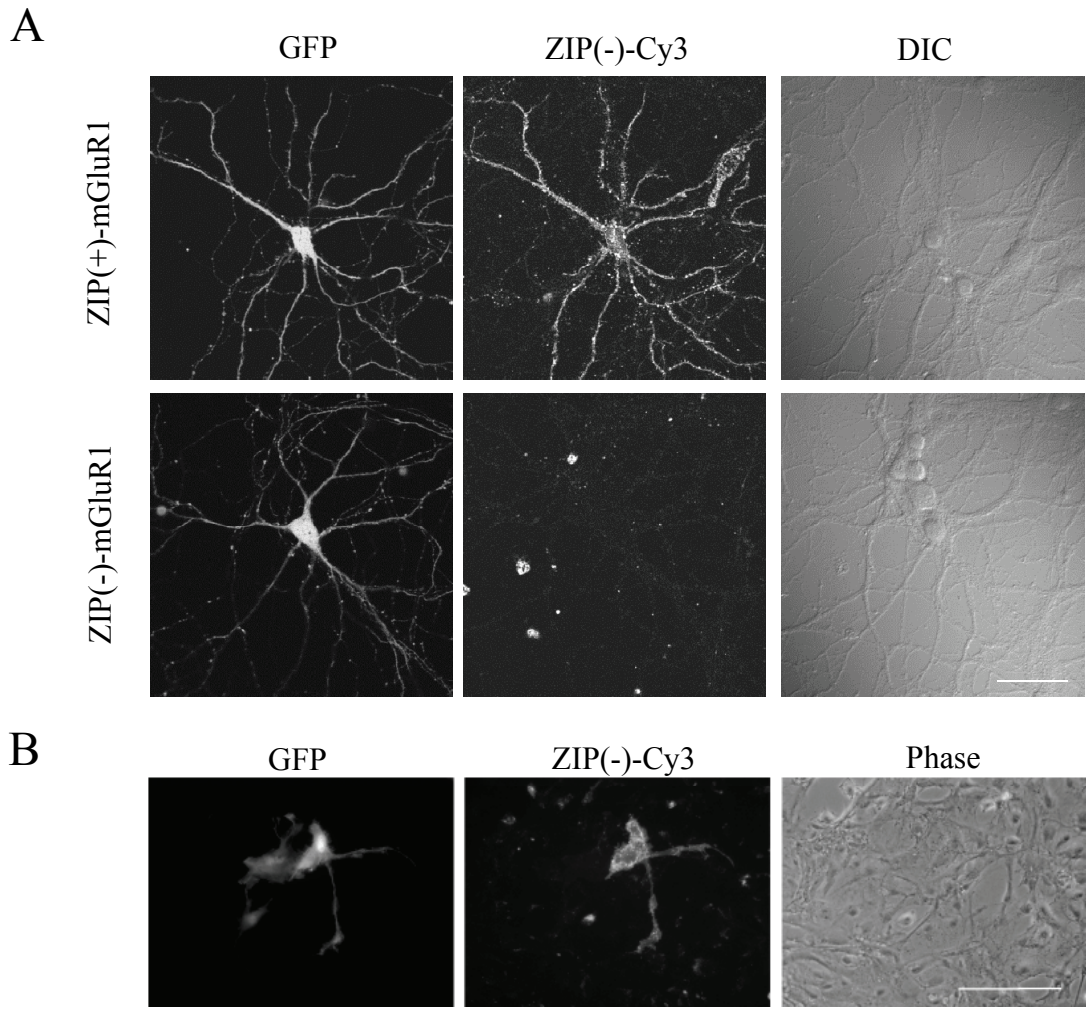

Fig. 4

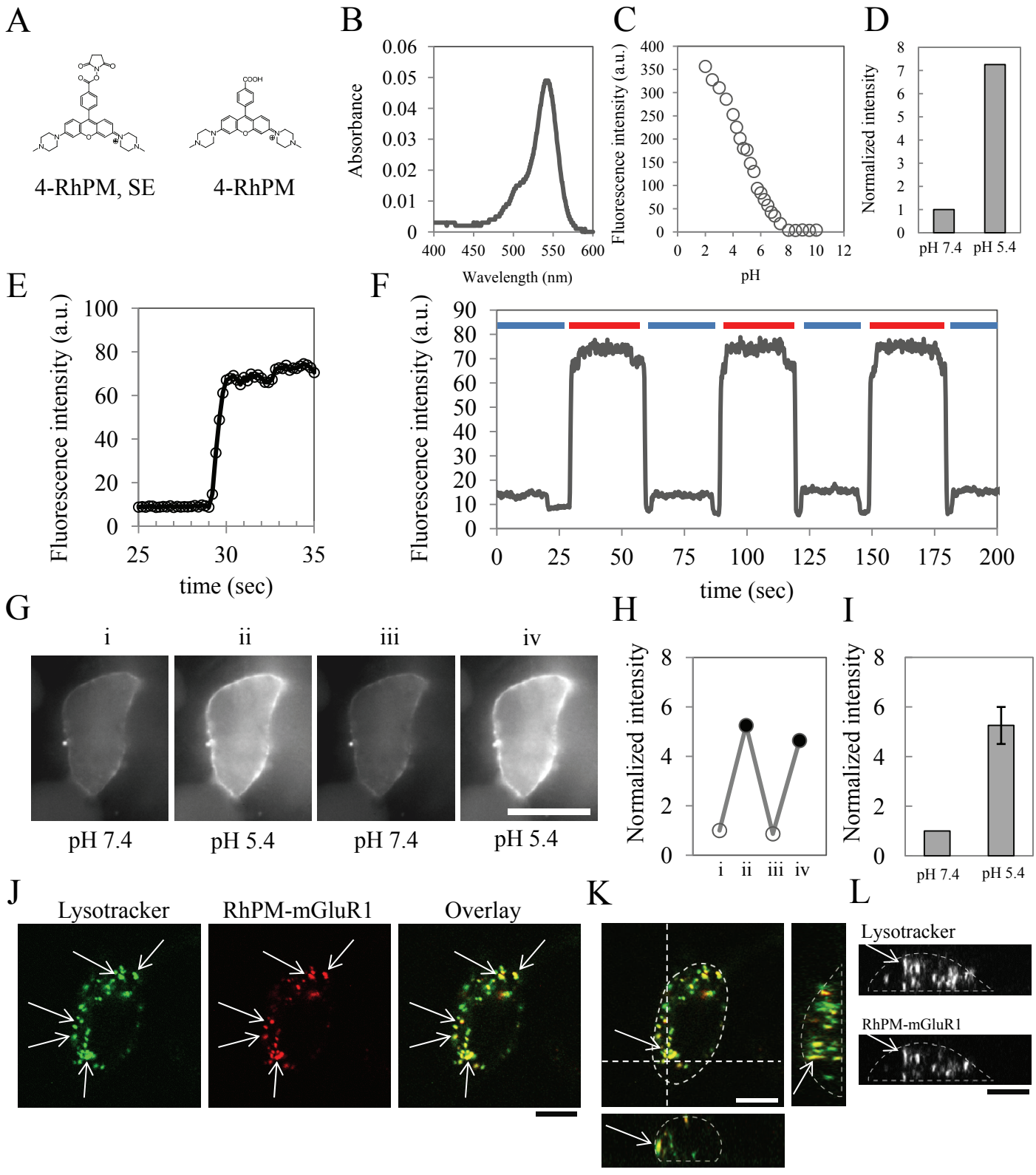
A
4-RhPM, SE
4-RhPM
B
Absorbance
Wavelength (nm)
C
Fluorescence intensity (a.u.)
pH
D
Normalized intensity
pH 7.4
pH 5.4
E
Fluorescence intensity (a.u.)
time (sec)
F
Fluorescence intensity (a.u.)
time (sec)
G
i
ii
iii
iv
pH 7.4
pH 5.4
pH 7.4
pH 5.4
H
Normalized intensity
i ii iii iv
I
Normalized intensity
pH 7.4
pH 5.4
J
Lysotracker
RhPM-mGluR1
Overlay
K
L
Lysotracker
RhPM-mGluR1

Fig. 5

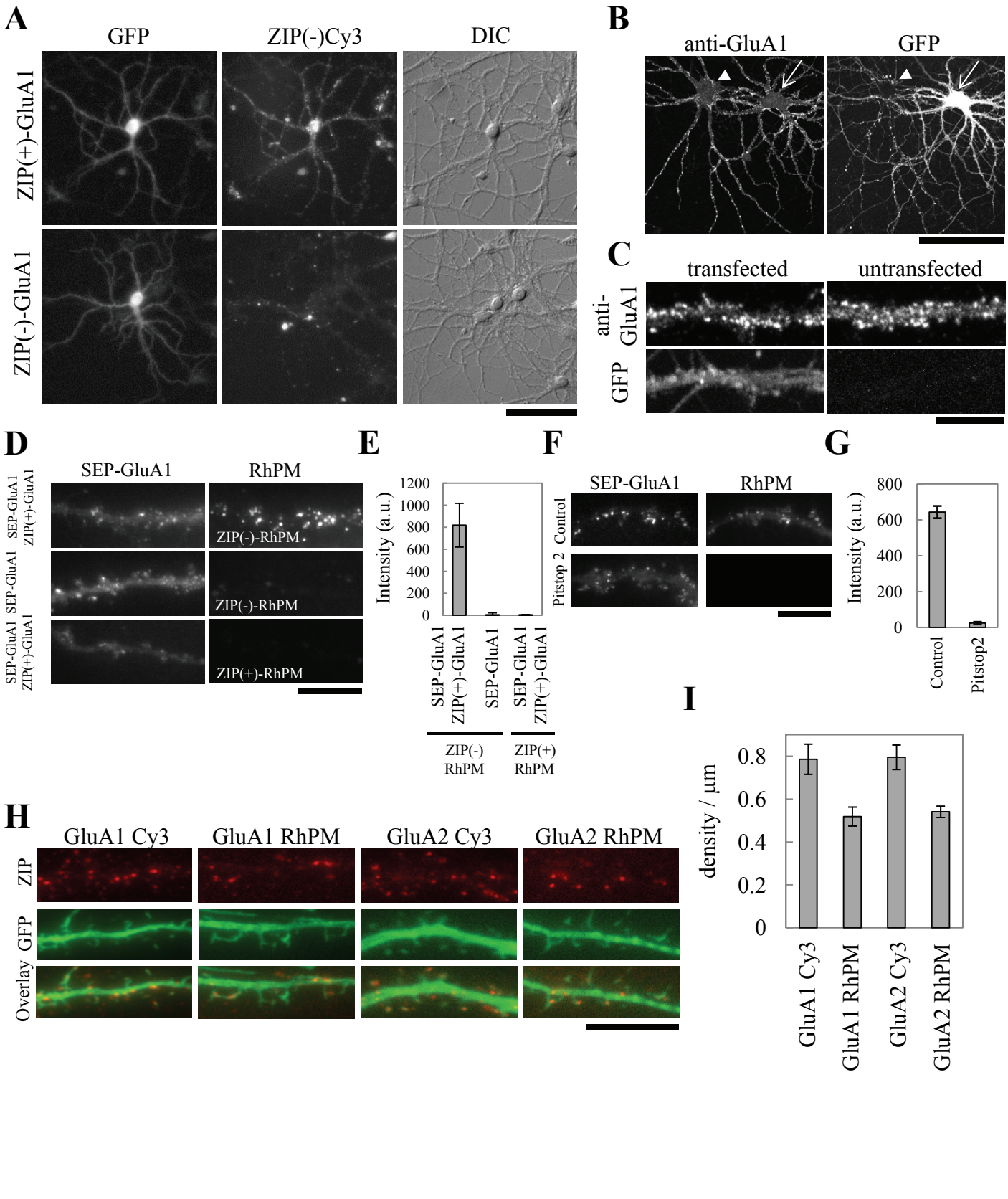
A
GFP
ZIP(-)Cy3
DIC
ZIP(+)-GluA1
ZIP(-)-GluA1
B
anti-GluA1
GFP
C
transfected
untransfected
anti-GluA1
GFP
D
SEP-GluA1
RhPM
SEP-GluA1 ZIP(+)-GluA1
SEP-GluA1
SEP-GluA1 ZIP(+)-GluA1
ZIP(-)-RhPM
ZIP(-)-RhPM
ZIP(+)-RhPM
E
Intensity (a.u.)
1200
1000
800
600
400
200
0
SEP-GluA1 ZIP(+)-GluA1
SEP-GluA1
SEP-GluA1 ZIP(+)-GluA1
ZIP(-) RhPM
ZIP(+) RhPM
F
SEP-GluA1
RhPM
Control
Pitstop 2
G
Intensity (a.u.)
800
600
400
200
0
Control
Pitstop2
H
GluA1 Cy3
GluA1 RhPM
GluA2 Cy3
GluA2 RhPM
ZIP
GFP
Overlay
I
density / µm
0.8
0.6
0.4
0.2
0
GluA1 Cy3
GluA1 RhPM
GluA2 Cy3
GluA2 RhPM

Fig. 6

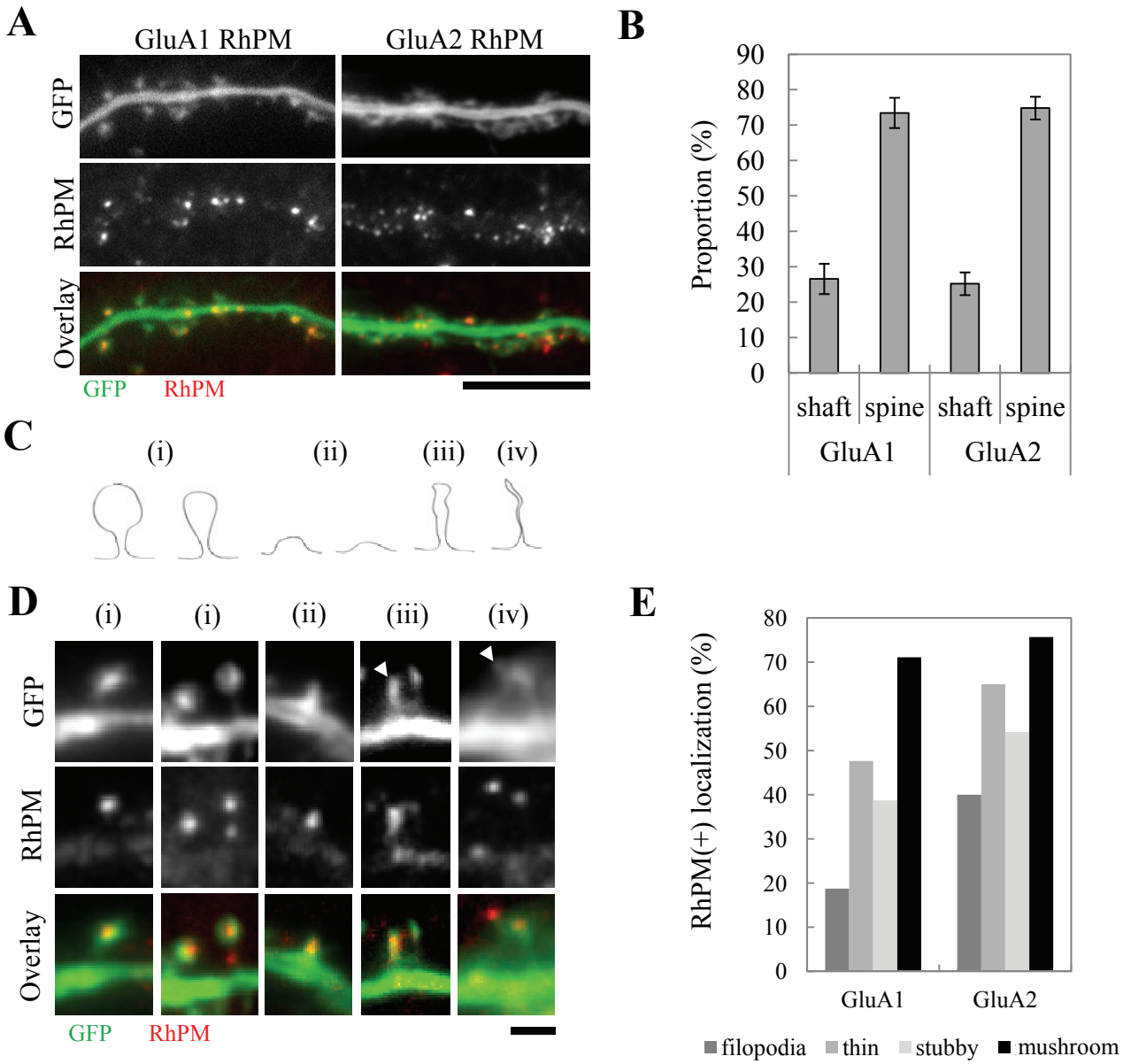
A
GluA1 RhPM
GluA2 RhPM
GFP
RhPM
Overlay
GFP RhPM
B
Proportion (%)
90
80
70
60
50
40
30
20
10
0
shaft spine shaft spine
GluA1 GluA2
C
(i) (ii) (iii) (iv)
D
(i) (i) (ii) (iii) (iv)
GFP
RhPM
Overlay
GFP RhPM
E
RhPM(+) localization (%)
80
70
60
50
40
30
20
10
0
GluA1 GluA2
filopodia thin stubby mushroom

Fig. 7

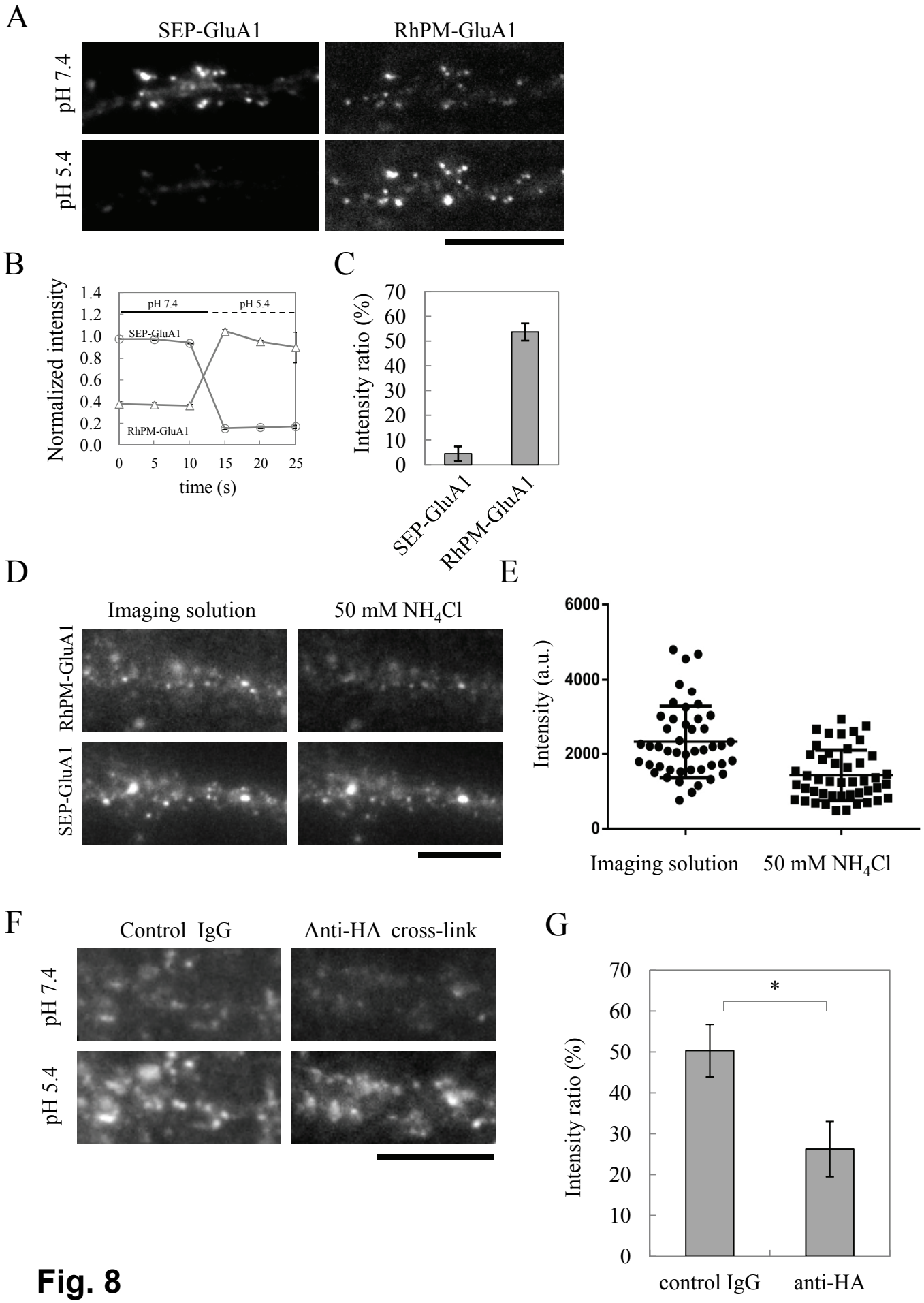
A
SEP-GluA1
RhPM-GluA1
pH 7.4
pH 5.4
B
Normalized intensity
pH 7.4
pH 5.4
SEP-GluA1
RhPM-GluA1
time (s)
C
Intensity ratio (%)
SEP-GluA1
RhPM-GluA1
D
Imaging solution
50 mM NH4Cl
RhPM-GluA1
SEP-GluA1
E
Intensity (a.u.)
Imaging solution
50 mM NH4Cl
F
Control IgG
Anti-HA cross-link
pH 7.4
pH 5.4
G
Intensity ratio (%)
*
control IgG
anti-HA

Fig. 8

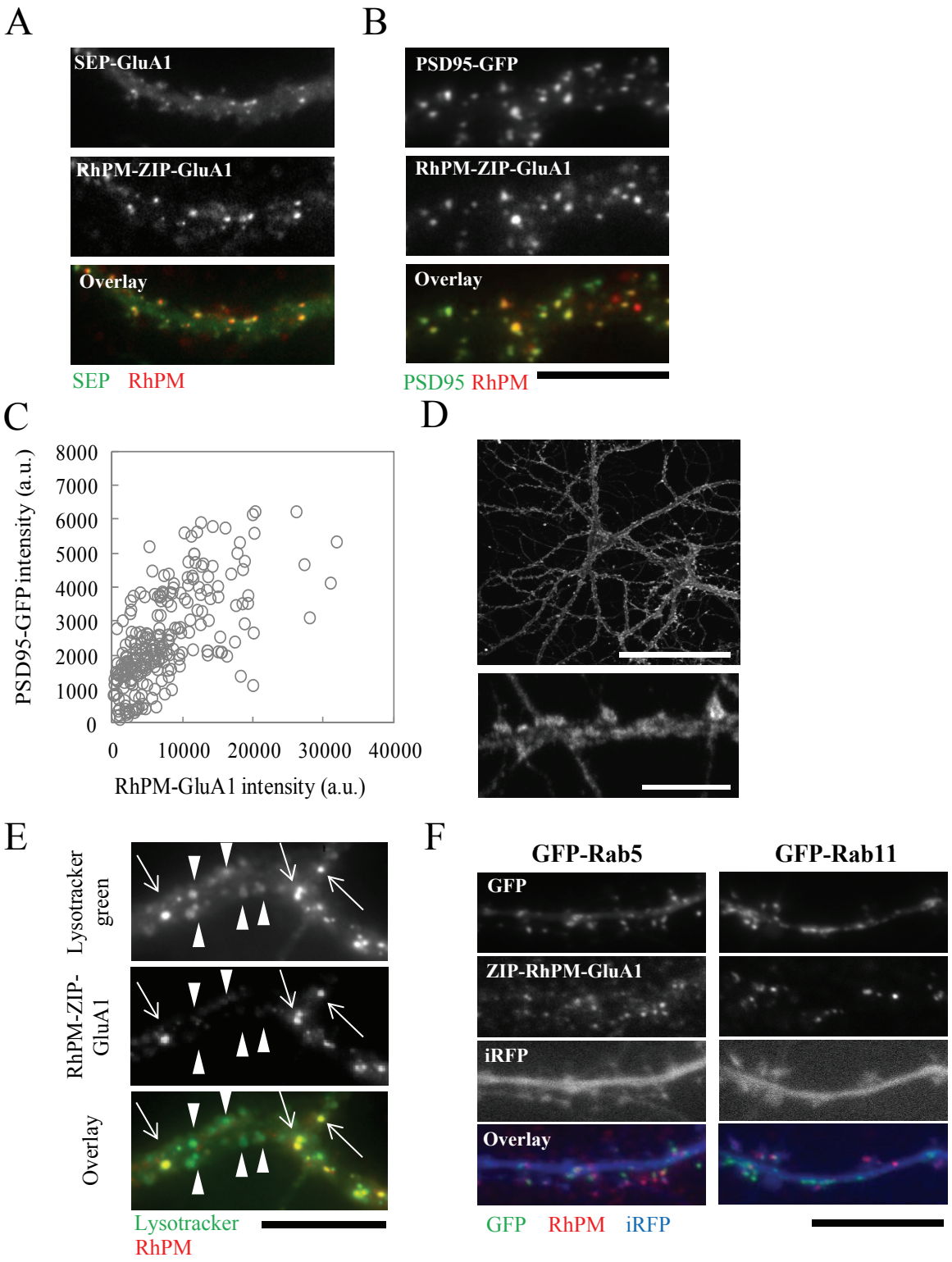
A
SEP-GluA1
RhPM-ZIP-GluA1
Overlay
SEP RhPM
B
PSD95-GFP
RhPM-ZIP-GluA1
Overlay
PSD95 RhPM
C
PSD95-GFP intensity (a.u.)
8000
7000
6000
5000
4000
3000
2000
1000
0
0
10000
20000
30000
40000
RhPM-GluA1 intensity (a.u.)
D
E
Lysotracker green
RhPM-ZIP-GluA1
Overlay
Lysotracker RhPM
F
GFP-Rab5
GFP-Rab11
GFP
ZIP-RhPM-GluA1
iRFP
Overlay
GFP RhPM iRFP

Fig. 9

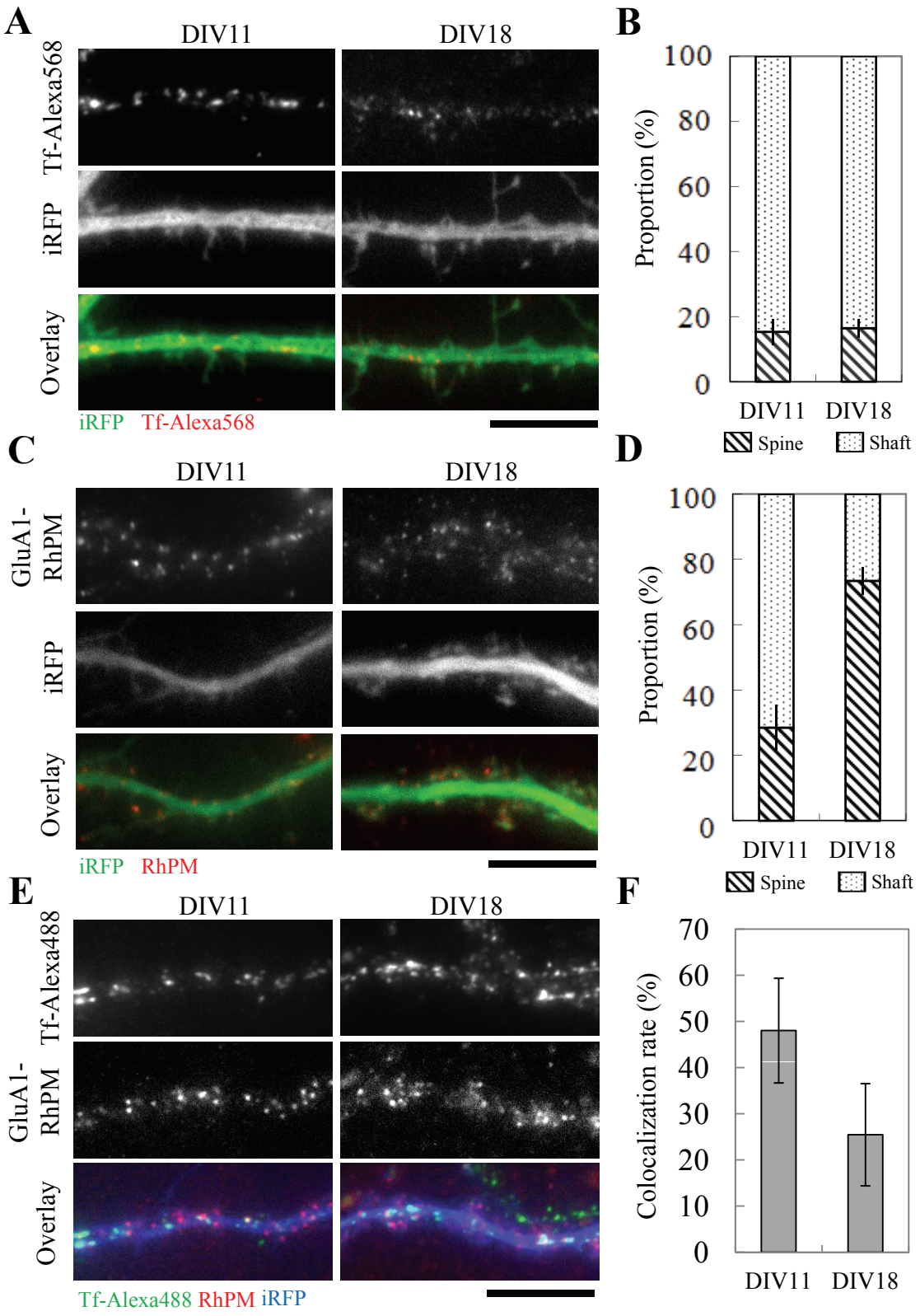
A
DIV11
DIV18
Tf-Alexa568
iRFP
Overlay
iRFP Tf-Alexa568
B
Proportion (%)
100
80
60
40
20
0
DIV11 DIV18
Spine
Shaft
C
DIV11
DIV18
GluA1-RhPM
iRFP
Overlay
iRFP RhPM
D
Proportion (%)
100
80
60
40
20
0
DIV11 DIV18
Spine
Shaft
E
DIV11
DIV18
Tf-Alexa488
GluA1-RhPM
Overlay
Tf-Alexa488 RhPM iRFP
F
Colocalization rate (%)
70
60
50
40
30
20
10
0
DIV11 DIV18

Fig. 10

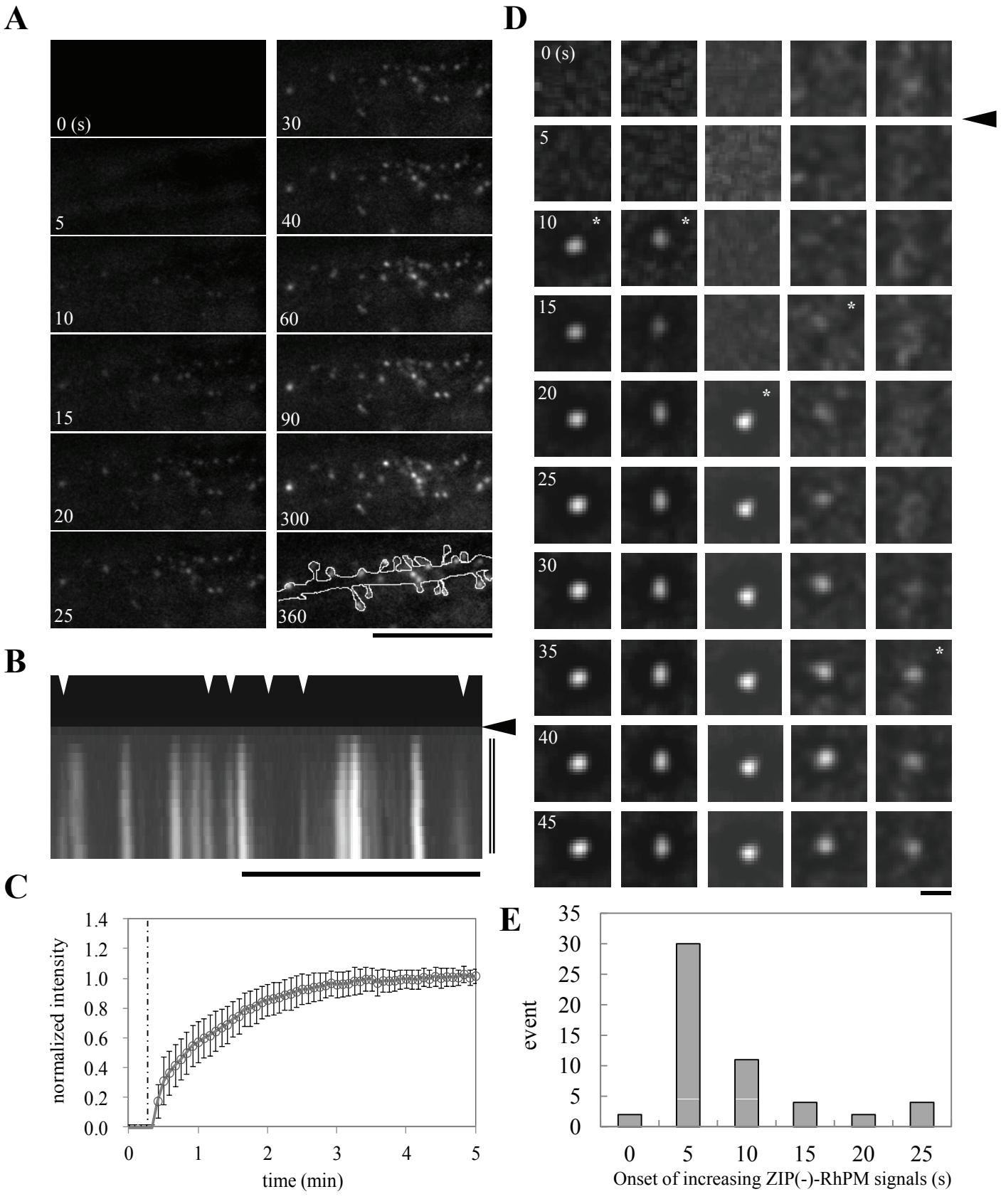
A
0 (s)
5
10
15
20
25
30
40
60
90
300
360
B
C
normalized intensity
time (min)
D
E
event
Onset of increasing ZIP(-)-RhPM signals (s)

Fig. 11

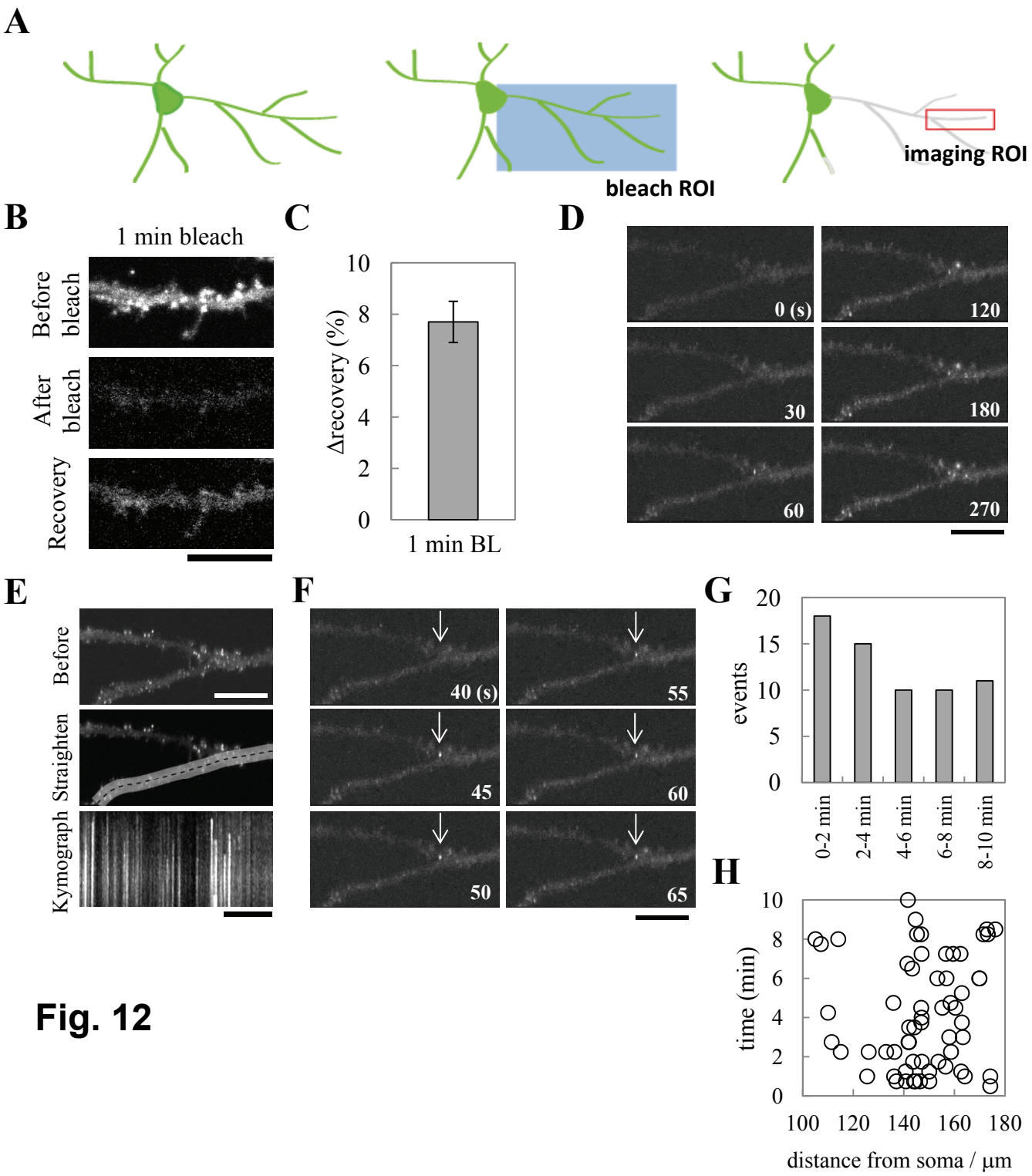
A
bleach ROI
imaging ROI
B
1 min bleach
Before bleach
After bleach
Recovery
C
Δrecovery (%)
10
8
6
4
2
0
1 min BL
D
0 (s)
120
30
180
60
270
E
Before
Straighten
Kymograph
F
40 (s)
55
45
60
50
65
G
events
20
15
10
5
0
0-2 min
2-4 min
4-6 min
6-8 min
8-10 min
H
time (min)
10
8
6
4
2
0
100
120
140
160
180
distance from soma / μm

Fig. 12

Table 1

Ligand		Tag		affinity		Ref.
	size(kDa)		size(kDa)	total	Kd IC50	
anti-HA-Antibodies	150	HA	2.2	152.2	10^{-9}- 10^{-11}	
n.a.		superecliptic phluorin	27	27	n.a.	11
α-bungarotoxin	8	nAchR a subunit	1.4	9.4	n.a. 1.8×10^{-5}	44
α-bungarotoxin	8	high affinity peptide 2	1.4	9.4	6.0×10^{-8} 2.0×10^{-9}	44
Rabies virus glycoprotein	3.2	nAc hR a subunit	1.4	4.6	8.6×10^{-6}	64
streptavidin	60	streptavidin binding peptide	4.2	64.2	2.5×10^{-8}	65
ZIP(-)	5.2	ZIP(+)	5.2	10.4	1.3×10^{-11}	19
GCN 4pLI	3.6	GCN 4pIL	3.6	7.2	n.a.	66
ICS	1.4	LEPB	1.6	3	2.1×10^{-6}	67
Halo tag ligand Alexa488	1.0	Halo tag	35.7	36.7	-	68
ReAsH/FlAsH	0.6/0.7	tetra-cistein (TC; CCPGCC)	0.7	1.3	1.3×10^{-3} / 2.4×10^{-4}	69

n.a., not applicable